SEMICONDUCTOR LASER BASED ON THERMOELECTROPHOTONICS

by

XIAOHANG LIU
B.S. Dalian University of Technology 2007

A dissertation submitted in partial fulfillment of the requirements
for the degree of Doctor of Philosophy
in the College of Optics and Photonics
at the University of Central Florida
Orlando, Florida

Summer Term
2014

Major Professor: Dennis G. Deppe

© 2014 Xiaohang Liu

ABSTRACT

This dissertation presents to our knowledge the first demonstration of a quantum well (QW) laser monolithically integrated with internal optical pump based on a light emitting diode (LED). The LED with high efficiency is operated in a thermoelectrophotonic (TEP) regime for which it can absorb both its own emitted light and heat. The LED optical pump can reduce internal optical loss in the QW laser, and enables monolithically integrated TEP heat pumps to the semiconductor laser. The design, growth and fabrication processes of the laser chip are discussed, and its experimental data is presented. In order to further increase the TEP laser efficiency the development of QDs as the active region for TEP edge emitting laser (EEL) is studied. The usage of QD as TEP laser's active region is significant in terms of its low threshold current density, low internal optical loss and high reliability, which are mainly due to low transparency in QD laser. The crystal growth of self-organized QDs in molecular beam epitaxial (MBE) system and characterization of QDs are mentioned. The design, growth, processing and fabrication of a QD laser structure are detailed. The characteristics of laser devices with different cavity length are reported. QD active regions with different amount of material are grown to improve the active region performance. Theoretical calculations based on material parameters and semiconductor physics indicate that with proper design, the combination of high efficiency LED in TEP regime with a QD laser can result in the integrated laser chip power conversion efficiency exceeding unity.

To my grandparents

ACKNOWLEDGMENT

First I am grateful to my advisor, Dr. Dennis Deppe, for offering me the great opportunity to work in the field of semiconductor lasers in his laboratory. Although he is one of the best scientists in this field, he still works closely with me and discusses details. The wisdom he shared in my learning process will benefit my research in the future.

I would like to thank my committee members, Dr. Eric Van Stryland, Dr. Aristide Dogariu and Dr. Michael Bass, for sparing their valuable time, interest and suggestions on my research. Dr. Bass's attitude in research is admirable. Without their help, I couldn't have made through my defense and thesis. Their passion about science and kindness in guidance of young researchers are what CREOL is about.

Many thanks go to Dr. Sabine Freisem for her patience and time in teaching me MBE. I want to thank Dr. Abdullah Demir and Dr. Guowei Zhao for their help with material growth, device fabrication and characterization. I also would like to thank other group members to go through this together with me. Much is owed to Rachel and Monica for their preparation of my paper works. I will always remember all my friends and colleagues in CREOL.

Last but not least, I would like to thank my parents and my wife. My parents barely know semiconductor or laser, but they love and support me for lifelong. My wife has been the continuous source of inspiration to me. This PhD degree is only another stop in the journey of my life, and my families are destined to share this wonderful trip with me. It is their company that makes every moment in my life meaningful.

TABLE OF CONTENTS

LIST OF FIGURES vii

LIST OF TABLES x

LIST OF ACRONYMS/ABBREVIATIONS xi

CHAPTER 1: INTRODUCTION 1

1.1 Semiconductor Light Emitting Diode in Thermoelectrophotonic Regime 1

1.2 Outline 5

CHAPTER 2: SEMICONDUCTOR LASER OPTICALLY PUMPED BY AN INTEGRATED LIGHT EMITTING DIODE 6

2.1 Introduction 6

2.2 Structure and Advantage of TEP Laser 10

2.3 TEP Laser Growth and Fabrication 16

2.4 TEP Laser Characterization 20

2.5 Summary 27

CHAPTER 3: TEP LASER WITH QUANTUM DOT ACTIVE REGION 28

3.1 Introduction 28

3.2 QD Active Material Growth 31

3.3 QD EEL Fabrication and Characterization 33

3.4 Possibility of Breaking Unity Efficiency in the Integrated Laser Chip with QDs as the TEP laser active region 42

3.5 Summary 48

CHAPTER 4: SUMMARY AND FUTURE WORK 50

LIST OF REFERENCES 51

LIST OF FIGURES

Figure 1-1 circuit diagram of an LED forward biased at VF ($VF < \hbar\omega ph$). Its current is $ILED$, it emits photons of energy $\hbar\omega ph$. 2

Figure 1-2 Band diagram of a forward biased LED. The dots stand for injected electrons and the circles stands for holes. They follow Fermi-Dirac distribution. 3

Figure 2-1 schematic of a typical semiconductor structure. QW active region locates in the center of WG and heavily doped p and n cladding. Two facets are coated with front and back mirrors. 7

Figure 2-2 Schematic illustration of the GaAs LED integrated with the semiconductor laser. The LED is electrically biased and optically pumps the laser waveguide and QW. The LED is designed to operate as thermoelectrophotonic heat pump, absorbing heat as it optically pumps the laser 11

Figure 2-3 p-mirror design with 10% AlGaAs and 67% AlGaAs mirrors, and its reflectivity vs. incident angle 12

Figure 2-4 n-mirror design with 10% AlGaAs and AlAs mirrors and its reflectivity vs. incident angle. The bottom mirrors have pass-band between 25 and 75 degree. 13

Figure 2-5: illustration of pass-bands 13

Figure 2-6: New design of n- mirror to be fabricated, the substrate of n mirror is etched off to increase its reflectivity at all angles 14

Figure 2-7 Fabrication processes of TEP laser. The wafer was fabricated into stripes with 120 μm wide stripes and 0.5 cm long cavity. The p and n ohmic contacts were formed for carrier injection. (a) n contact of Ge/Au, (b) p contact and mirror of Ag/Au, (c) pattern for wet etching, (d) shallow mesa was formed using citric acid, (e) deposit aluminum oxide for current blocking, (f) wider Cr/Au contact 18

Figure 2-8 Photolumenescence measured at 300 K and 77 K from the as-grown epitaxial sample. The HeNe pump light is absorbed in the GaAs LED region. The GaAs emission is shown at 870 nm at 300 K (dashed curve), and 830 nm at 77 K (solid curve). The GaAs spontaneous emission pumps the QW, and the QW emits at 980 nm at 300 K (dashed curve) and at 930 nm at 77 K (solid curve). 21

Figure 2-9 Electroluminescence measured from the chip at two different bias levels. The below threshold level at 0.5 A shows both the GaAs emission and the QW emission. At 2 A only laser emission from the QW occurs. 24

Figure 2-10 Light vs. current curve from the chip measured CW from both facets. Driving the LED electrically optically pumps the QW laser, which produces the laser emission shown in the inset. The stripe dimensions are 120 μm × 0.5 cm 25

Figure 2-11 optical power vs. current data of two samples 665C (blue) and 665B (red), and their sizes are 120 μm × 0.5 cm and 50 μm × 0.5 cm, respectively. 26

Figure 3-1 Density of states in active region of Bulk, QW and QD structure 29

Figure 3-2 Development of EEL threshold current density 30

Figure 3-3 Stranski-Krastanow (SK) growth mode in forming quantum dots 32

Figure 3-4 AFM scan of QD test growth. The growth of InGaAs on GaAs was terminated after the quantum dots formed. The density of the QDs is 2×10^{10} cm^{-2} (left). The lateral size, height of the QDs are 500 Å, and 60 Å respectively 33

Figure 3-5 Schematic of QD broad area symmetric waveguide laser diode. The cladding layers are $Al_{0.35}Ga_{0.65}As$. The waveguide layer is $Al_{0.15}Ga_{0.85}As$. The active region uses the same QD structure as the test growth, a single layer of InGaAs QDs. The QD wafer is fabricated into 120 μm wide and 0.5 cm long laser diodes 34

Figure 3-6 Fabrication procedure of the QD laser, the wafer was fabricated into stripes with 120 μm wide stripes and 0.5 cm long cavity. The p and n ohmic contacts were formed for carrier injection. 35

Figure 3-7 Photoluminescence spectra of a laser structure with the active region of 1 InGaAs QDs at 300 K and 77 K. The active region emitted at 985 nm with a FWHM of 92meV at 300K (dash line), and at 946nm with a FWHM of 58meV at 77K (solid line). 36

Figure 3-8 L-I curves for p-up mounted QD laser diodes at room-temperature for CW operation of devices with 100 μm stripe width, and 0.3, 0.5, and 1 cm cavity length. The inset shows the threshold current and threshold current density. 37

Figure 3-9 Electroluminescence spectra at room-temperature for different injected current density 0.1 A, 0.3 A, and 0.4 A below and above threshold 38

Figure 3-10 PL spectra of a laser structure with 15 Å InGaAs at 300 K and 77 K. The active region emitted at 894 nm with a FWHM of 26.4 meV at 300K (dash line), and at 846 nm with a FWHM of 20.8 meV at 77 K (solid line). The line width indicated the active region was a QW 39

Figure 3-11 PL spectra of a laser structure with 17.5 Å InGaAs at 300 K and 77 K. The active region emitted at 899 nm with a FWHM of 24.6 meV at 300 K (dash line), and at 852 nm with a FWHM of 22.3 meV at 77 K (solid line). The bump between 860 nm and 900 nm are probably the transition from QW into quantum dots 41

Figure 3-12 PL spectra of a laser structure with 25 Å InGaAs at 300 K and 77 K. The active region emitted at 960 nm with a FWHM of 41.8 meV at 300 K (dash line), and at 1010 nm with a FWHM of 82.8 meV at 77 K (solid line). The stronger emission and narrower linewidth indicate the sizes of quantum dots are more uniform and the gain is larger. The red-shift of

peak wavelength is due to the larger size of quantum dots making separation of ground states of electrons and holes larger. 42

Figure 3-13 single optical mode in QD laser waveguide structure, the confinement factor in the active region is 0.0102 44

Figure 3-14 Simulated power conversion efficiency of integrated chip 47

Figure 3-15 Power conversion efficiency of integrated chip (left) and LED (right) of a device with 0.4 cm cavity length 48

LIST OF TABLES

Table 2-1 quantum efficiency estimate of LED with PL results 23

Table 3-1 loss and threshold calcualtion with different cavity length 46

LIST OF ACRONYMS/ABBREVIATIONS

AFM	Atomic Force Microscopy
CW	Continuous Wave
EEL	Edge-Emitting Laser
EL	Electroluminescence
LED	Light Emitting Diode
MBE	Molecular Beam Epitaxy
PCE	Power Conversion Efficiency
PL	Photoluminescence
QD	Quantum Dot
QW	Quantum Well
SSL	Short-period Super Lattice
TEP	Thermoelectrophotonic
WL	Wetting Layer
WPE	Wall-Plug Efficiency

CHAPTER 1: INTRODUCTION

1.1 Semiconductor Light Emitting Diode in Thermoelectrophotonic Regime

Semiconductor light emitting diodes (LEDs) can operate in a thermoelectrophotonic (TEP) regime for which their power conversion efficiency may exceed unity. The TEP effect occurs in a spontaneously emitting light emitting diode when the drive voltage to the LED is less than the photon energy [1,2,3,4]. Under this bias condition each spontaneously radiated photon carries energy at the amount equal to the energy gap of the semiconductor, while the energy drawn from the external voltage source to generate the photon remains less than the photon energy. The net energy difference between that drawn from the external source and that of the radiated photon is made up by heat absorption from the crystal lattice. Some light emitting diode materials, such as bulk GaAs, can reach very high internal quantum efficiency greater than 99% [5]. Under these conditions net heat absorption becomes possible by the LED, and the LED achieved self-cooling [6,7,8,9,10,11,12,13]. While the TEP regime physics that can produce greater than unity power conversion efficiency have been understood for some time, only recently has it been demonstrated in an LED at very low bias and output power [14,15].

The physical mechanisms of the self-cooling with the possibility of refrigeration and waste heat recovery in p-n junction light emitters were recognized just after the demonstration of high efficiency light emission from GaAs diodes [1]. As illustrated in Figure 1-1, when an externally applied voltage V_F is applied to a light emitting diode this forward bias will result in emission of photons with energy $\hbar\omega_{ph}$ and a current I_{LED} in the LED.

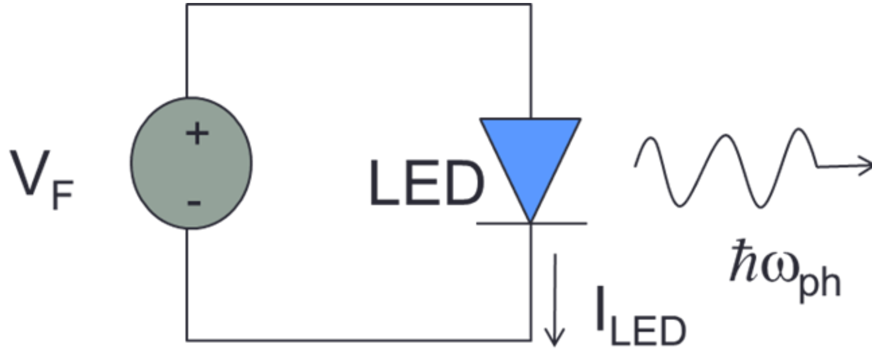

Figure 1-1 circuit diagram of an LED forward biased at V_F ($V_F < \hbar\omega_{ph}$). Its current is I_{LED}, it emits photons of energy $\hbar\omega_{ph}$.

Input electrical power drawn from the applied source is

$$P_i = V_F \cdot I_{LED} \tag{1.1}$$

The output optical power drawn from the applied source is given by a radiated power

$$P_o = \hbar\omega_{ph}(I_{LED}/q) \cdot \eta_{inj}\eta_{int}\eta_{ex} \tag{1.2}$$

where η_{inj} is the injection efficiency, η_{int} is the internal efficiency, η_{ex} is the extraction efficiency of LED. The wall plug efficiency of LED is

$$\eta_{wp} = (\hbar\omega_{ph}/qV_F) \cdot \eta_{inj}\eta_{int}\eta_{ex} \tag{1.3}$$

With sufficient efficiencies for internal recombination and light extraction, the wall plug efficiency can be approximated by,

$$\eta_{wp} \approx \hbar\omega_{ph}/qV_F \tag{1.4}$$

when the applied voltage is less than emission photon energy ($V_F < \hbar\omega_{ph}/q$), the efficiency could be exceed unity, and the output P_o will exceed the input P_i. The remaining power $P_o - P_i$ is due to heat drawn from the thermal contact and heat sink. Figure 1-1 illustrates the circuit diagram of such an LED device.

The physics of LED in TEP regime is illustrated in Figure 1-2. A GaAs LED is sandwiched by AlGaAs p and n cladding. The LED is forward biased with external voltage V_F ($qV_F < \hbar\omega_{ph}$). The dots in n AlGaAs cladding standing for electrons and the circles in p AlGaAs cladding standing for holes follow the Fermi-Dirac distribution. The low level bias voltage ($qV_F < \hbar\omega_{ph}$) causes preferential injection of electrons and holes with high energy at the energetic tips of Fermi tails (or the "hot" electrons and holes) into the junction, then the electrons and holes recombine and emit photons, and this preferential injection of hot carriers causes cooling of the electron gases near the junction.

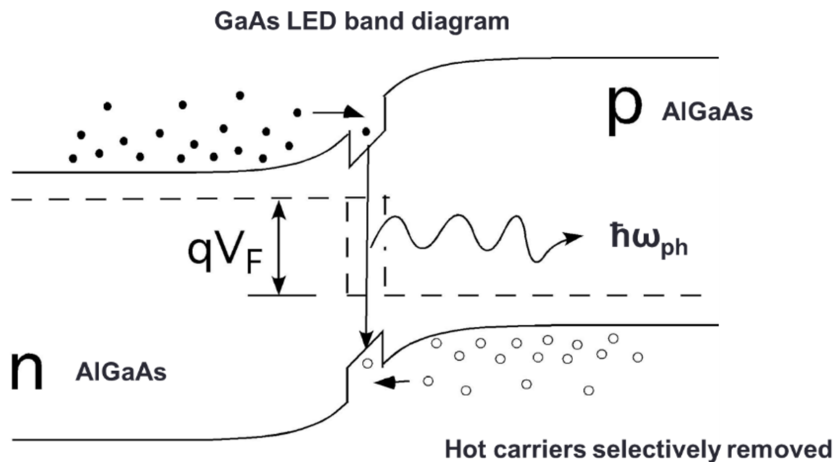

Figure 1-2 Band diagram of a forward biased LED. The dots stand for injected electrons and the circles stands for holes. They follow Fermi-Dirac distribution.

The dominance of diffusion current due to hot electrons and holes in the weakly forward biased p-n junction selectively remove of only the highest energy carriers effectively cools the electron gas in the region next to the junction, causing the electron gas temperature to fall below the semiconductor lattice temperature. The phonons in the lattice then reheat the electrons at a rate set by the thermal conductivity of the material, and the temperature difference between the electron gas and the lattice of the semiconductor crystal. The heat in crystal lattice is absorbed by electron gas and transferred into photon emission, and therefore the semiconductor LED is self-cooled. The LED uses electrical power to pump heat from their own semiconductor lattice to the outgoing optical field [15].

The experimental demonstration of the greater than unity efficiency so far suffers major drawbacks for applications, mainly because the LED has been demonstrated requires extracting the spontaneous emission from the semiconductor chip. This light extraction suffers from Snell's law and a small escape cone from the LED chip. For example, with semiconductor' refractive index (~3.5) much smaller than that of air (~1), only the light within a small angle (~16°) can be extracted. On the other hand, a laser that operates with greater than unity efficiency would be much more useful and quite likely to be a technological revolution, because of its directional emission and high extraction efficiency. Such devices could produce usable power levels while operating in the self-cooling regime. They are of interest for high power laser operation, especially applications such as laser fusion, where the heat generation due to laser pumping may otherwise be enormous. However, as opposed to an LED, a diode laser requires a voltage drive that exceeds the laser photon energy to reach carrier inversion, while the TEP regime needed for

greater than unity efficiency in an LED requires a voltage drive that is less than the photon energy. Therefore it does not appear possible that a diode laser operating alone can break the unity efficiency barrier.

1.2 Outline

This thesis first introduces an LED optical pump monolithically integrated with a semiconductor laser in chapter two. The LED operates in a self-cooling regime that can produce heat absorption, offering the possibility of heat pump action. The design, growth and fabrication processes of the laser chip are discussed, and the experimental data is presented. The optimized semiconductor laser structure is expected to have low internal loss and high efficiency. The calculation of TEP laser maximum efficiency also concludes that in order to reach high power conversion efficiency, low threshold and low internal loss of the laser active region are necessary. Therefore chapter three is mainly focused on QDs with low internal loss and threshold to be the active region of TEP laser. The physics of QD laser's low transparency is explained. A literature review of threshold and internal loss of semiconductor EEL is presented. Self-organized QDs growth in MBE system is introduced. The characterization of these QD active regions is demonstrated. A QD EEL with symmetric waveguide is designed, grown and fabricated. The characteristics of laser devices with different cavity length are reported. Simulations based on semiconductor physics and material parameters investigate the possibility of the laser chip exceeding unity power conversion efficiency by using QDs as the active region.

CHAPTER 2: SEMICONDUCTOR LASER OPTICALLY PUMPED BY AN INTEGRATED LIGHT EMITTING DIODE

2.1 Introduction

Semiconductor laser was first discovered in 1962 [16,17,18,19], and it was a breakthrough invention in industry. In the late 1970s, double-hetereostructure lasers with reduced threshold continuous wave (CW) emission were developed [20,21]. The development of metallorganic chemical vapor deposition (MOCVD) and molecular beam epitaxy (MBE) enabled laser designers to control the crystal growth accuracy to the level of atomic layer. Large aperture laser devices greatly enhanced power output from single lasers. Output powers above several watts were demonstrated [22,23,24,25,26,27]. The most important criterion for high power laser is described by its wall plug efficiency [28,29,30,31], which is the electrical-to-optical power conversion efficiency. The maximum efficiency of commercial device is about 70% [32,33,34]. Other features including small temperature sensitivity, high reliability through operating wavelength and better beam quality are also desirable [35].

Figure 2-1 shows a typical QW semiconductor laser structure. The active region of QW is located in a large optical cavity. It reduces the optical power density thus eliminating catastrophic optical damage at the end facets of the laser. The carrier confinement layer is separated from the waveguide, in order to facilitate high carrier injection efficiency.

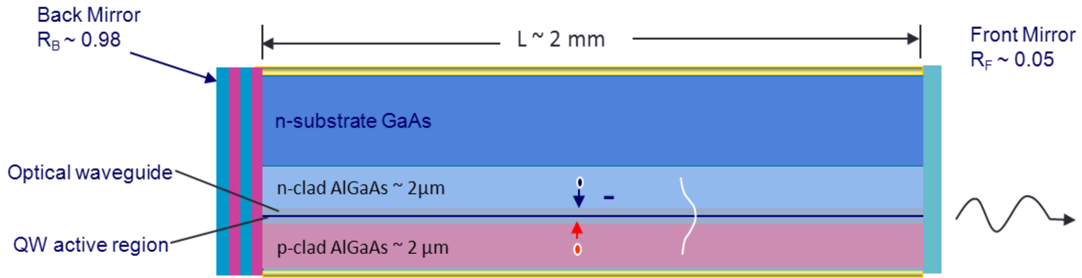

Figure 2-1 schematic of a typical semiconductor structure. QW active region locates in the center of WG and heavily doped p and n cladding. Two facets are coated with front and back mirrors.

The wall plug efficiency, η_{wp} of an edge-emitting laser is given as the product of internal quantum efficiency η_{inj}, optical extraction efficiency η_{ex} and electrical conversion efficiency η_{elec}:

$$\eta_{wp} = \frac{P_o}{P_i} = \eta_{inj}\eta_{ex}\eta_{elec} \tag{2.1}$$

All the efficiency terms are interrelated. By reducing doping in the cladding region and broadening the waveguide optical efficiency will improve. However, lightly doped claddings will introduce larger series resistance which will cause electrical efficiency to degrade and broader waveguides will cause η_i to drop [36]. Hence careful optimization is required to maximize wall-plug efficiency. In semiconductor lasers, since the carrier density is clamped above threshold, the η_i value can approach 100%. The wall plug efficiency expression and output power can be further elaborated as:

$$\eta_{wp} = \eta_{inj} \frac{\ln(\frac{1}{R_F})}{2\alpha_i \mathrm{L} + \ln(\frac{1}{R_F R_B})} \frac{\hbar\omega_{ph}(I - I_{th})}{q(I^2 R_s + IV_J)} = \eta_{inj} \frac{\ln(\frac{1}{R_F})}{2\alpha_i \mathrm{L} + \ln(\frac{1}{R_F R_B})} \frac{\hbar\omega_{ph}(J - J_{th})}{q(J^2 \rho_s + JV_J)}$$

(2.2)

$$P_o = \eta_{inj} \frac{\ln(\frac{1}{R_F})}{2\alpha_i \mathrm{L} + \ln(\frac{1}{R_F R_B})} \frac{\hbar\omega_{ph}(I - I_{th})}{q} = \eta_{inj} \frac{\ln(\frac{1}{R_F})}{2\alpha_i \mathrm{L} + \ln(\frac{1}{R_F R_B})} \frac{\hbar\omega_{ph}(J - J_{th})WL}{q}$$

(2.3)

in which the input power is $P_i = q(J^2\rho + JV_J)WL$, L is the laser cavity length, W is the stripe width, $\hbar\omega_{ph}/q$ is the voltage related to the radiated photon energy, V_J is the forward voltage at the p-n junction active region with, I is the electrical current, I_{th} is the threshold current, and R_s is the electrical series resistance and α_i is the internal loss.

It is necessary to keep the optical losses as low as possible in order to achieve high power output from a semiconductor laser [37]. The internal optical loss is a combination of scattering loss and free carrier absorption. Scattering loss is mainly due to inhomogeneity of the material and heterointerfaces in the structure. It can be eliminated by improving crystal growth quality and careful choice of material. Free carrier absorption occurs when electron or hole absorbs photons and makes transition within the same band. Phonons are involved in this transition for conservation of momentum. Free carrier absorption rises with free carrier density, and it is the dominant loss mechanism in laser diodes. The free carrier absorption is composed of active region loss and cladding loss. The active region loss depends on the threshold current which is

largely determined by the material properties and heterostructure of the laser active region. The cladding loss comes from the p and n doped claddings. These losses can be expressed as:

$$\alpha_{active} = \frac{\Gamma_m}{\Delta z}(\sigma_e n_{act,th} + \sigma_h p_{act,th}) \tag{2.4}$$

$$\alpha_{clad} = \Gamma_{nclad}\sigma_e n_{clad} + \Gamma_{pclad}\sigma_h p_{clad} \tag{2.5}$$

where α_{clad} is the internal loss, Γ_{nclad} and Γ_{pclad} are optical mode confinement factor in p and n cladding. $n_{act,th}$ and $p_{act,th}$ are the carrier densities of electrons and holes in the active region. n_{clad} and p_{clad} are the carrier densities of electrons and holes in the cladding. $\sigma_e = 3 \times 10^{-18}\ cm^2$ and $\sigma_h = 7 \times 10^{-18}\ cm^2$ are their free carrier absorption cross sections, which vary with semiconductor material and wavelength. The scattering cross-section for holes in GaAs are usually several times bigger than that for electrons. Δz is the active region thickness used to normalize overlap of optical mode and active region.

The maximum wallplug efficiency depends on operating level or injection level and intrinsic device parameters. The product of cavity length and internal loss in (2.2) sets limit on PCE and there is always a drop in its maximum resulting from the increase of cavity length [38]. The output optical power increases linearly with cavity length L. Therefore to achieve high power while maintaining high efficiency we need to carefully optimize doping and waveguide combination to reduce the internal loss but keep laser resistance low at the same time. There is always a trade-off in optimization: reducing modal overlap causes modal gain to drop, and lightly doped waveguide introduces higher resistance for injected carriers.

In next section a novel design of a semiconductor laser monolithically integrated with a light emitting diode is introduced. It shows that through optically pumping, we can break the inter-dependence between optical loss and electrical resistance. We expect substantial reduction in internal loss and longer cavity thus greatly enhancing the efficiency and output power.

2.2 Structure and Advantage of TEP Laser

Modern semiconductor technology enables the monolithic integration of an LED that can operate in the TEP regime with greater than unity efficiency with a semiconductor laser, for which the LED acts as an optical pump as well as a TEP heat pump to the laser. In fact, as we show below, this type of integration eliminates the need to extract the LED emission from the chip, and instead benefits from Snell's law. Our calculations in the next chapter indicate that the combination could result in an integrated laser chip for which the laser optical output power exceeds the chip's electrical input power.

Figure 2-2 demonstrates a schematic of the integrated laser chip. The LED is either bulk GaAs or AlGaAs and semiconductor laser uses a single InGaAs QW. Both the LED and laser are clad between two mirrors. The p-type mirror is comprised of two p-type pairs of quarter-wave layers of $Al_{0.1}Ga_{0.9}As/Al_{0.67}Ga_{0.33}As$, followed by phase matching p-type $Al_{0.1}Ga_{0.9}As$ and p^+ GaAs contact layers and a post-growth deposited Ag mirror. The Ag mirror also serves as an electrical p-contact to the LED. The n-type mirror is based on 16 quarter wave pairs of $Al_{0.1}Ga_{0.9}As/AlAs$. The semiconductor laser uses $Al_{0.3}Ga_{0.7}As$ cladding layers, a 0.5 μm thick

GaAs waveguide layer, and a 60 Å $In_{0.2}Ga_{0.8}As$ QW active region. All layers of the laser except the QW active layer are doped n-type at ~10^{17} cm^{-3}. Above the laser is grown a p-n bulk LED with an undoped active thickness of 1.5 μm and cladding p-n $Al_{0.1}Ga_{0.9}As$ electrical injection layers. The two mirror stacks trap the spontaneous emission of the LED, which undergoes photon recycling and ultimately absorption in the laser waveguide [39]. The integrated laser is p-down mounted to BeO heat sink.

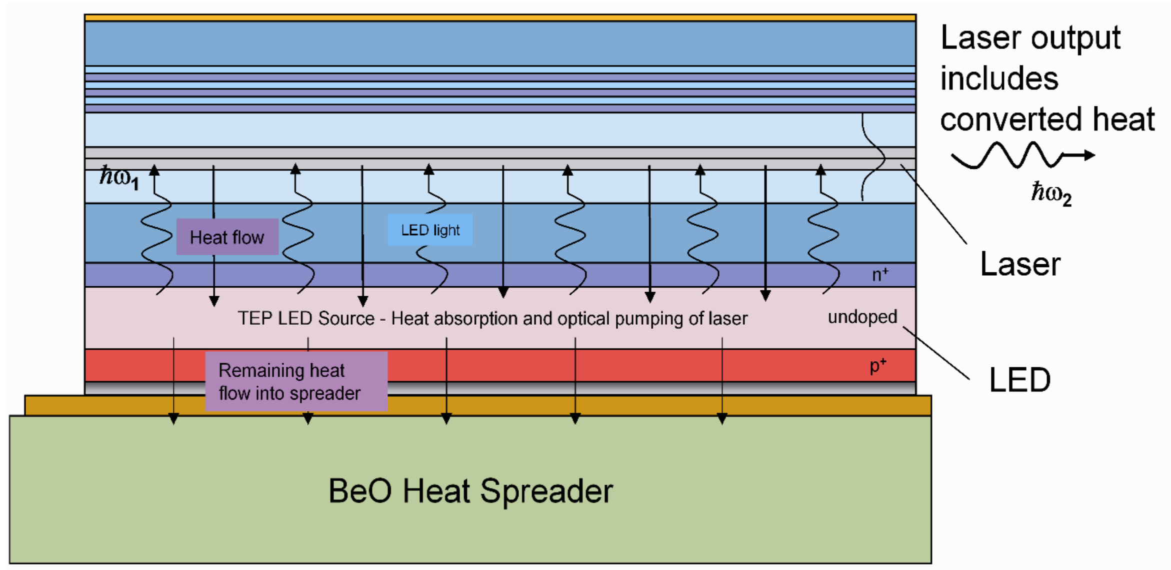

Figure 2-2 Schematic illustration of the GaAs LED integrated with the semiconductor laser. The LED is electrically biased and optically pumps the laser waveguide and QW. The LED is designed to operate as thermoelectrophotonic heat pump, absorbing heat as it optically pumps the laser

The mirror layers are nominally designed to capture the GaAs LED emission in the laser waveguide. The coupling of the bulk LED light by the laser waveguide is mainly due to off-normal spontaneous emission, because of the significant solid angle in the off-normal direction.

At large off-normal angle the mirror interfaces become totally internally reflecting and traps the LED spontaneous emission in the semiconductor laser waveguide. Thus in contrast to the attempts to extract the spontaneous emission from the bulk LED, the spontaneous emission is instead trapped and coupled internally. The electrical contacting uses electron transport through the GaAs substrate and laser to electrically bias the GaAs bulk LED. Figure 2-3 shows a simulated top mirror structure and its reflectivity vs. incidence angle. The large imaginary part of silver refractive index produces a high reflectivity for p mirror in all angles (above 99%). The mirror thickness was designed for LED emission peak wavelength,

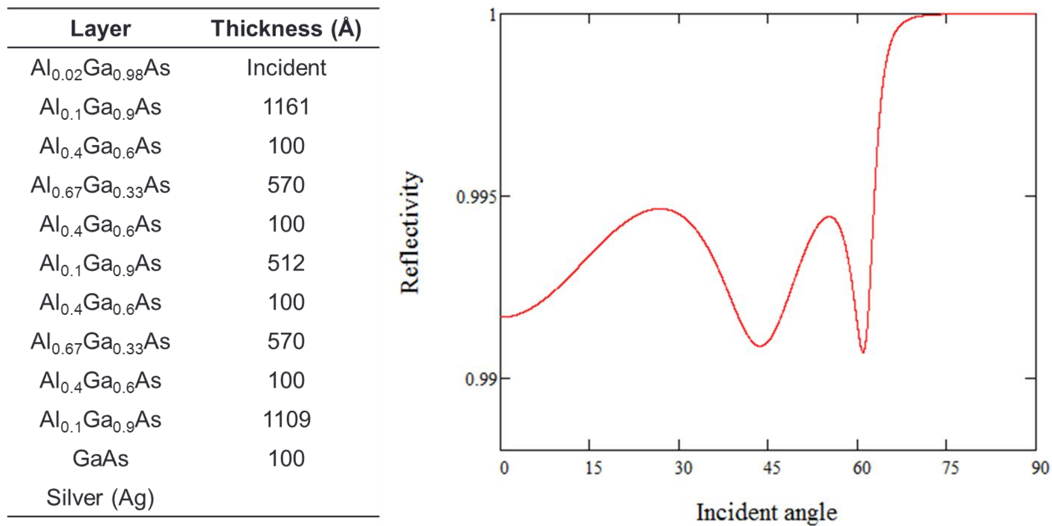

Layer	Thickness (Å)
$Al_{0.02}Ga_{0.98}As$	Incident
$Al_{0.1}Ga_{0.9}As$	1161
$Al_{0.4}Ga_{0.6}As$	100
$Al_{0.67}Ga_{0.33}As$	570
$Al_{0.4}Ga_{0.6}As$	100
$Al_{0.1}Ga_{0.9}As$	512
$Al_{0.4}Ga_{0.6}As$	100
$Al_{0.67}Ga_{0.33}As$	570
$Al_{0.4}Ga_{0.6}As$	100
$Al_{0.1}Ga_{0.9}As$	1109
GaAs	100
Silver (Ag)	

Figure 2-3 p-mirror design with 10% AlGaAs and 67% AlGaAs mirrors, and its reflectivity vs. incident angle

The bottom mirrors structure and reflectivity vs. incident angle are plotted in Figure 2-4, but the bottom mirrors have pass-band between 25 and 75 degree. This problem will lead to the escape of off-normal emission of LED.

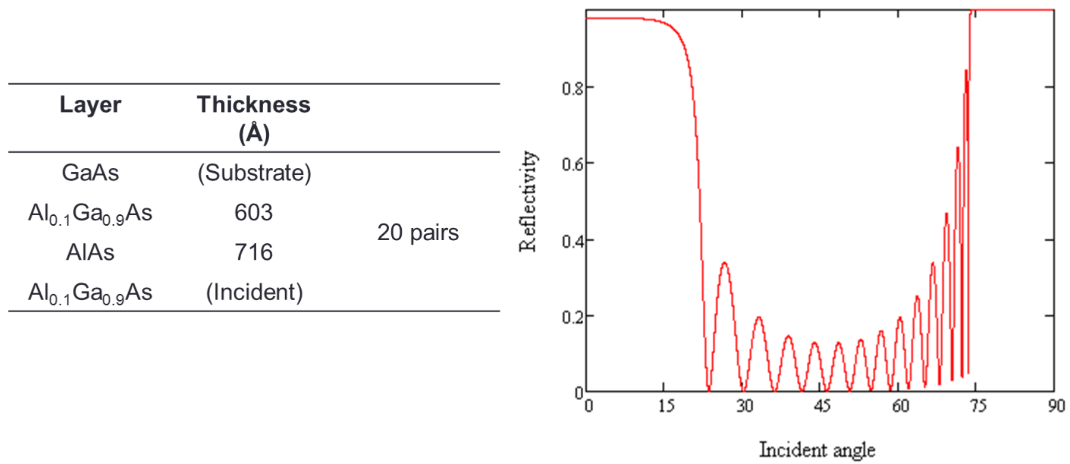

Layer	Thickness (Å)	
GaAs	(Substrate)	
$Al_{0.1}Ga_{0.9}As$	603	20 pairs
AlAs	716	
$Al_{0.1}Ga_{0.9}As$	(Incident)	

Figure 2-4 n-mirror design with 10% AlGaAs and AlAs mirrors and its reflectivity vs. incident angle. The bottom mirrors have pass-band between 25 and 75 degree.

Figure 2-5 illustrates the problem of pass-band in n mirror.

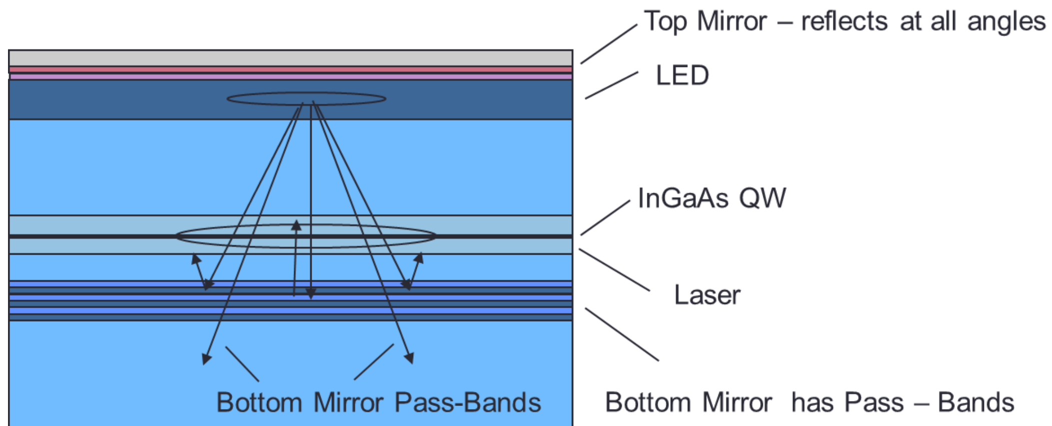

Figure 2-5: illustration of pass-bands

In order to trap all LED light within device another structure of bottom mirror with “air substrate” is designed. Figure 2-6 shows its structure and calculated reflectivity. The bottom mirror with etched-off GaAs substrate produces an air-semiconductor interface and reflects LED

emission from all angles with reflectivity of more than 99.5%. The off-normal reflection is mainly due to internal reflection.

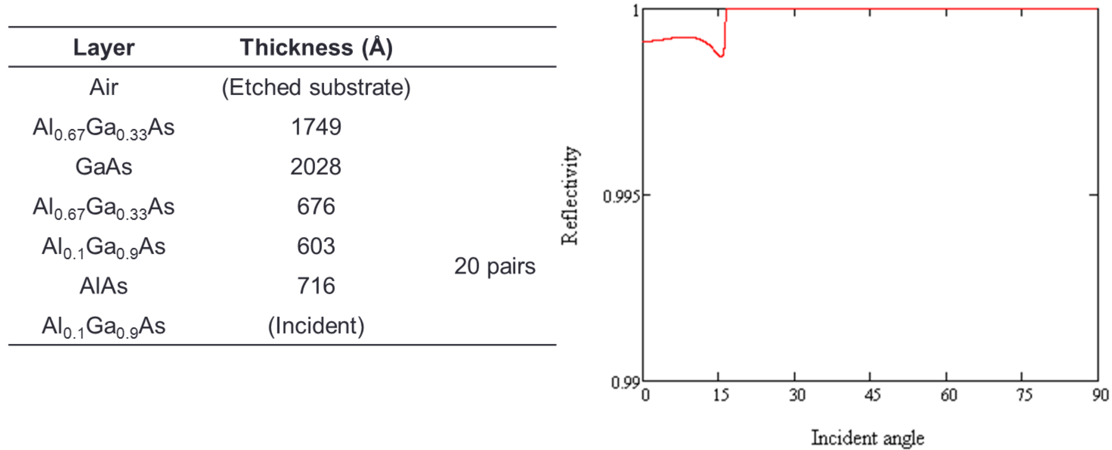

Layer	Thickness (Å)	
Air	(Etched substrate)	
$Al_{0.67}Ga_{0.33}As$	1749	
GaAs	2028	
$Al_{0.67}Ga_{0.33}As$	676	
$Al_{0.1}Ga_{0.9}As$	603	20 pairs
AlAs	716	
$Al_{0.1}Ga_{0.9}As$	(Incident)	

Figure 2-6: New design of n- mirror to be fabricated, the substrate of n mirror is etched off to increase its reflectivity at all angles

Under ideal operation, self-cooling occurs in the LED due to its bias condition and high internal quantum efficiency. This self-cooling depends on the thickness of the LED and can reach several hundred watts per square centimeter. The LED is operating at a lower internal temperature than the laser, and this difference in operating temperature will cause heat flow into the LED from its surrounding crystal regions, including from the laser. The estimate fraction of spontaneous emission that can be coupled to the laser in an ideal design is close to 100%. The spontaneous transfer is increased by a modified radiation pattern from the LED due to its internal absorption. Our calculations also indicate that the amount of lost spontaneous emission can be minimized by increasing the thickness of the laser waveguide to give close to 100% total absorption of the LED light by the laser.

The power conversion efficiency of the LED is,

$$\eta_{PCE,TEP} = \frac{P_{TEP}}{P_{Source}} = \frac{\hbar\omega_{LED}/q}{J\rho_c + V_{J,LED}} \eta_{inj}\eta_{int}\eta_{op,TEP-Laser} \tag{2.6}$$

where $\eta_{op,TEP-Laser}$ is the LED light coupled to the laser, the optically pumped laser absorbs TEP LED light and emits light with its photon energy. The power conversion efficiency of laser can be expressed as,

$$\eta_{PCE,laser} = \frac{P_{Laser}}{P_{TEP}} = \frac{\hbar\omega_{Laser}}{\hbar\omega_{TEP}} \frac{P_{TEP} - P_{TEP,th}}{P_{TEP}} \frac{ln(1/R_F)}{\ln(1/R_F) + \ln(1/R_B) + 2\alpha_i L} \tag{2.7}$$

in which $\frac{\hbar\omega_{Laser}}{\hbar\omega_{TEP}}$ is the quantum defect term, equal to the ratio of the photon energy. It is beneficial to make emission photon energy of LED and laser as close as possible but too little difference between the two may reduce the LED emission in laser active region and the coupling efficiency. Therefor the power conversion efficiency of the integrated TEP laser chip is the product of LED efficiency and laser efficiency,

$$\eta_{PCE,TEPlaser} = \frac{P_{Laser}}{P_{source}} = \frac{P_{TEP}}{P_{source}} \frac{P_{Laser}}{P_{TEP}} =$$

$$\frac{\hbar\omega_{TEP}/q}{J\rho_c + V_{J,LED}} \eta_{op,TEP-Laser} \eta_{\mathrm{inj}} \eta_{int,TEP} \frac{\hbar\omega_L}{\hbar\omega_{TEP}} \frac{J - J_{th}}{J} \frac{ln(1/R_F)}{\ln(1/R_F) + \ln(1/R_B) + 2\alpha_i L} \tag{2.8}$$

in which J_{th} is the current density of the LED and is the threshold power needed for lasing. The current density of laser and TEP LED can be related by,

$$J_{th} = q \frac{P_{TEP,th}}{\hbar\omega_{TEP}} = \frac{J_{th,Laser}}{\eta_{op,TEP-Laser}\eta_{int,TEP}} \tag{2.9}$$

Therefore the power conversion efficiency of the integrated chip is dependent on injected current density J. From formula (2.8) it can be concluded that due to optical pumping, the laser benefit from the optical pumping instead of electrical injection. This reduces the internal absorption loss that mainly caused by heavily p and n doping of the laser's cladding layers. The LED pumping of the laser also enables elimination of the p-doping and associated holes injection, which also reduces internal optical loss and increase injection efficiency, because the free carrier absorption of holes is more than twice of that of electrons. The low free carrier absorption helps increase the efficiency of the laser and the output power of the device can be improved by making the cavity length longer without sacrificing the power conversion efficiency. The monolithic integration has additional benefits and can be adapted to other devices as well, such as solar cells or possibly electronics for waste heat conversion.

2.3 TEP Laser Growth and Fabrication

The TEP laser was monolithically grown in Varian Gen II Solid Source molecular beam epitaxial (MBE) system located at the College of Optics and Photonics, the University of Central Florida. It is equipped with 12 source ports. The atomic flux from each source cells are controlled by the temperature setting of those cells. Deposition of each source material is controlled by shutters in front of the source cells. The advantage of MBE includes high-quality epitaxial growth of III-V compound semiconductor, sharp interfaces, pure material and precise

control of thickness composition and doping. The high vacuum system maintains background pressure lower than 10^{-11} Torr and the pressure during the growth around 10^{-6} Torr.

The TEP laser was grown on n^+ GaAs (100) substrate. In the structure described in Figure 2-2, the growth started with n-type $Al_{0.1}Ga_{0.9}As$/AlAs quarter wavelength bottom DBR mirror, followed by $Al_{0.3}Ga_{0.7}As$ n cladding layer, a 0.5 μm thick GaAs waveguide with a 60 Å $In_{0.2}Ga_{0.8}As$ QW as active region, and then another $Al_{0.3}Ga_{0.7}As$ n cladding. After the growth of GaAs or AlGaAs LED, two p-type pairs of quarter-wave layers of $Al_{0.1}Ga_{0.9}As$/ $Al_{0.67}Ga_{0.33}As$ and phase matching p-type $Al_{0.1}Ga_{0.9}As$ and p^+ GaAs contact layers were grown on top. The n-type doping was silicon (Si), and the p-type doping was beryllium (Be). The LED and laser were sandwiched between top and bottom mirrors. In order to get high quality AlGaAs material in laser structure and LED active region, their growth temperature was raised to 705 ℃, and the relatively low growth temperature ~580 ℃ is used to grow precise thickness of mirror. The growth temperature of InGaAs QW is ~540 ℃ to avoid indium desorption. The relatively high temperature of growing AlGaAs material will suppress oxygen incorporation with aluminum and eliminate non-radiative recombination.

The TEP laser wafer was processed into broad area laser diodes using the existing III-V material processing technology. The fabrication procedure of quantum dot laser wafer is demonstrated in Figure 2-7. In (a), 120 μm wide p metal stripes consist of 1500 Å silver and 500 Å gold (Ag/Au) on top of the fresh epi-structure. In order to form these metal stripes, we span a layer of positive photo-resist AZ 5214 on the wafer surface at 4000 rpm for 40 seconds, then baked the wafer at 90 ℃ for 15 minutes in an oven. With a mask designed with of stripe

openings, we were able to make patterns though contact UV lithography. After exposure in UV light for 10 seconds, the wafer was developed in AZ 726 MIF developer for 45 sec. Before the metal deposition, to remove the native oxide layer surface, the wafer was dipped in the mixture of hydrogen chloride and deionized water, (HCl:DI, 1:1 in volume) for 5 sec. 1500 Å silver and 500 Å gold were deposited in thermal evaporator. By immersing the wafer in acetone, one could perform p metal lift-off.

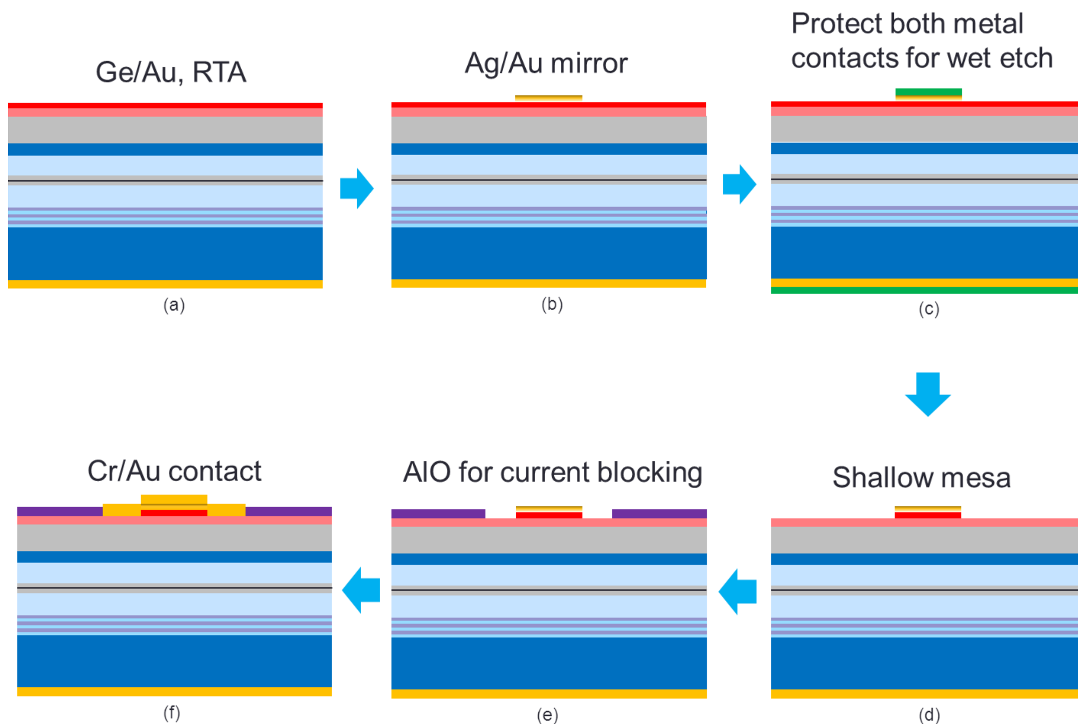

Figure 2-7 Fabrication processes of TEP laser. The wafer was fabricated into stripes with 120 μm wide stripes and 0.5 cm long cavity. The p and n ohmic contacts were formed for carrier injection. (a) n contact of Ge/Au, (b) p contact and mirror of Ag/Au, (c) pattern for wet etching, (d) shallow mesa was formed using citric acid, (e) deposit aluminum oxide for current blocking, (f) wider Cr/Au contact

In order to protect p metal contact and epi-structure, we put the wafer epi-side down on a piece of glass slide spread with photo-resist, and then hard baked them at ~110 ℃ for 10 minutes in the oven, as shown in (c). The back side (n-side) of the wafer is etched in a mixture of sulfuric acid, hydrogen peroxide and deionized water (H_2SO_4: H_2O_2: DI H_2O, 4:1:1 in volume) for 20 minutes. The thickness of damaged region in MBE crystal growth was etched off by ~20 μm. Therefore the n-metal would have better contact with semiconductor substrate and device resistance would be reduced. The wafer was then cleaned with acetone, isopropyl alcohol and deionized water thoroughly and dipped into (HCl: DI H_2O, 1:1 in volume) for 5 sec before the n-contact metallization. The n metal contact using 200 Å germanium and 1500 Å gold (Ge/Au) were deposited in thermal evaporator. After the rapid thermal annealing (RTA) at 360 ℃ for 30 sec, the n metal alloyed with GaAs and Ohm contact was formed.

Lithographically patterned photo-resist stripes were formed to cover p- metal and the n-metal was protected by putting it on glass slide spread with photo-resist. They were baked together at 90 ℃ for 10 minutes. In a mixture of citric acid and hydrogen peroxide (CA: H_2O_2, 4:1 in volume), the wafer was etched for 55 sec to form a shallow etched mesa ~1000 Å on the p side. Citric acid is selective in etching AlGaAs material depending on aluminum composition, and it stopped etching at 30% AlGaAs layer. We etched off the heavily doped top layers in this step to achieve current confinement. To remove photo-resist, the wafer was cleaned with acetone, isopropyl alcohol and deionized water after the etching.

As shown in Figure 2-7 (e), p-contact was covered with 270 μm wide photo-resist stripes, then a layer of 3500 Å aluminum oxide was deposited by e-beam evaporation followed by lift-

off with acetone with ultrasonic cleaner. The use of aluminum oxide produced better current confinement. The region next to p-metal without aluminum oxide was designed for better thermal management. Another p-metal of 200 Å chromium and 1500 Å gold (Cr /Au) were deposited on top of the first p-metal. This metal was also to make better contact and prevent the gold-tin (Au/Sn) solder from going into the semiconductor for the p-down mounted device.

2.4 TEP Laser Characterization

Figure 2-8 shows photoluminescence from the as-grown structure at 300 K and 77 K. The epitaxial structure was excited using a 15 mW HeNe laser operated at 0.6328 μm with a 1 mm diameter excitation spot. The HeNe laser pump was mainly absorbed in the LED layers closer to the sample surface. The GaAs LED active region then also pumped the laser waveguide and QW in photoluminescence. The comparison was made between the 300 K and 77 K photoluminescence to estimate the GaAs emission efficiency. The emission spectra, taken from the epitaxial surface show the GaAs LED emission peak at 0.87 μm at 300 K and 0.83 μm at 77 K, and the $In_{0.2}Ga_{0.8}As$ QW emission of the laser at 0.98 μm at 300 K and 0.93 μm at 77 K. This emission is spectrally modified by the vertical cavity structure of the upper and lower mirrors, but clearly shows both the GaAs LED emission and the $In_{0.2}Ga_{0.8}As$ QW emission. Because of the thicknesses of the LED layers including the p and n $Al_{0.1}Ga_{0.9}As$ injection layers, the $In_{0.2}Ga_{0.8}As$ QW emission can be assumed to result from only optical pumping by the GaAs LED emission towards the substrate.

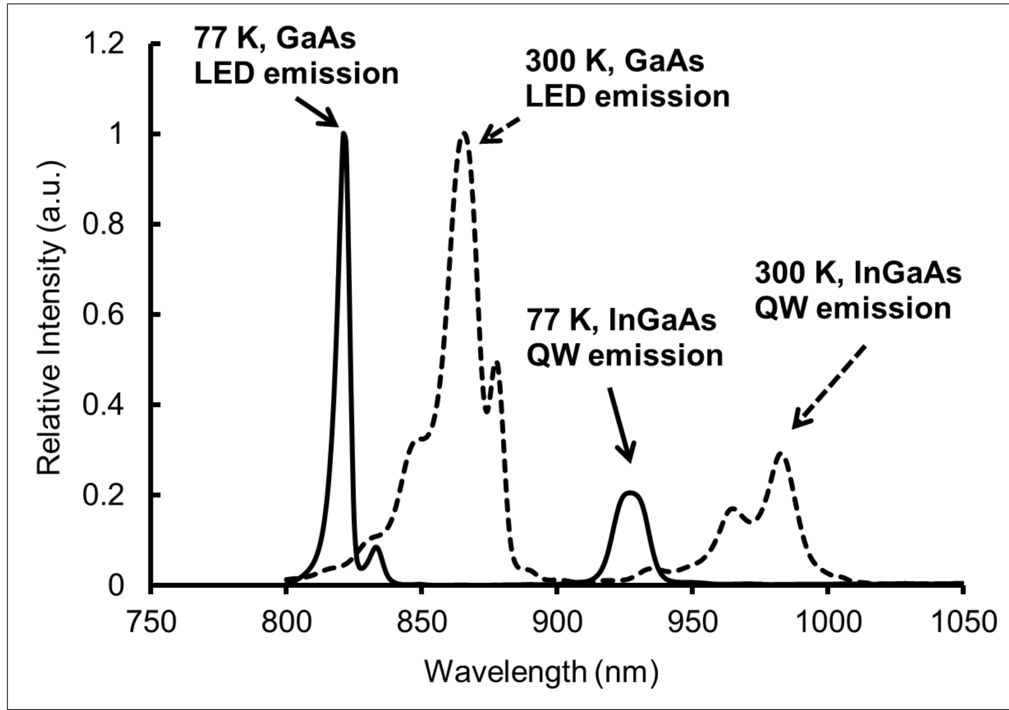

Figure 2-8 Photolumenescence measured at 300 K and 77 K from the as-grown epitaxial sample. The HeNe pump light is absorbed in the GaAs LED region. The GaAs emission is shown at 870 nm at 300 K (dashed curve), and 830 nm at 77 K (solid curve). The GaAs spontaneous emission pumps the QW, and the QW emits at 980 nm at 300 K (dashed curve) and at 930 nm at 77 K (solid curve).

By comparing the integrated emission intensity at 77K and room temperature, and assuming 100% internal quantum efficiency at 77K, the internal quantum efficiency of the He-Ne laser pumped GaAs LED region at room temperature can be estimated by

$$\eta_{int} \approx I(300K)/I(77K) \tag{2.1}$$

in which $I(300K)$ and $I(77K)$ are LED photoluminescence intensity at 300K and 77K. With rate equation of the LED

$$\frac{dn}{dt} \approx \frac{J}{qW_{LED}} - Bnp - An \quad (2.2)$$

where q is the electronic charge, n is the electron concentration in the LED bulk, p is the hole concentration, J is the pump current density. In the case of photoluminescence samples, it can be estimated by the electron-hole pairs generated by optical pumping of HeNe laser,

$$J = \frac{q}{\hbar\omega_{HeNe}} \frac{P_{HeNe}}{A_{HeNe}} \quad (2.3)$$

$\hbar\omega_{HeNe}$ is the photon energy of HeNe laser, P_{HeNe} and A_{HeNe} are the power and spot size of HeNe laser. W_{LED} is the LED thickness, B is the radiative bimolecular recombination rate, and A is the defect nonradiative recombination rate, one can estimate the quantum efficiency with injected carrier density p and

$$\eta_{int} \approx \frac{B(300K)np}{B(300K)np + A(300K)n} \approx \frac{B(300K)p}{B(300K)p + A(300K)} \quad (2.4)$$

The calculated quantum efficiency and estimate heat pump capacity of all photoluminescence samples is shown in Table 2-1. The high internal quantum efficiency is consistent with other measurements on surface-free bulk GaAs. The shaded devices are eligible to be heat pump and the maximum estimated heat pump capacity is 264 W/cm^2 when the injection is 6×10^{17} cm^{-3}, corresponding to 2000 A/cm^2, which is the operating current of typical lasers. GaAs p doped LED has low efficiency due to defects, undoped AlGaAs with low Al composition LED's efficiency is about 95% when injection is at 1×10^{18} cm^{-3}. The reason that it's not as high as GaAs is because AlGaAs LED active region has more impurities such as oxygen, and the corresponding non-radiative recombination is higher.

Table 2-1 quantum efficiency estimate of LED with PL results

Sample	LED material	η_{QE} when p=n=6e17 cm^{-3} (~ 2000 A/cm^2)	Estimated heat pump capacity of 0.5 μm LED (W/cm^2)
635	GaAs undoped	96%	243
637	GaAs undoped	45%	-26
646	GaAs Be 5E17	7%	-228
651	GaAs Be 5E17	13%	-157
653	GaAs undoped	99.6%	264
655	2%AlGaAs undoped	89%	206
656	2%AlGaAs undoped	89%	206
661	2%AlGaAs undoped	94%	233
663	GaAs Be 8E17	8%	-222
665	2%AlGaAs undoped	90%	212
672	GaAs undoped	96%	243
674	GaAs undoped	96%	243

The wafer was fabricated into broad area laser diodes using procedure described in last section. Electrical contacting to the GaAs LED was through the Ag mirror/contact placed on the upper p-side of the integrated chip, and through the Ge/Au alloyed contact formed on the GaAs n^+ substrate. The electron current of the n-side is therefore passed through the laser waveguide and QW. The laser and LED spectral emission were measured driving the chip quasi-continuous-wave without heat sinking, simply probing the chip placed on a metal contact. No soldering or other heat sinking was used, so that the 40 ms electrical pulses of the quasi-continuous-wave operation cause some heating of the chip. Figure 2-9 shows the electroluminescence spectra measured from one facet of the chip both below and above threshold. While GaAs LED emission could be measured below threshold, only $In_{0.2}Ga_{0.8}As$ QW lasing was measured above threshold.

In fact the GaAs LED injection current density at threshold of 333 A/cm^2 is far below the estimated value of 9000 A/cm^2 needed to invert the electron-hole population of the GaAs LED. If the GaAs LED region did become inverted, its thickness would easily support lasing end-to-end in the GaAs LED.

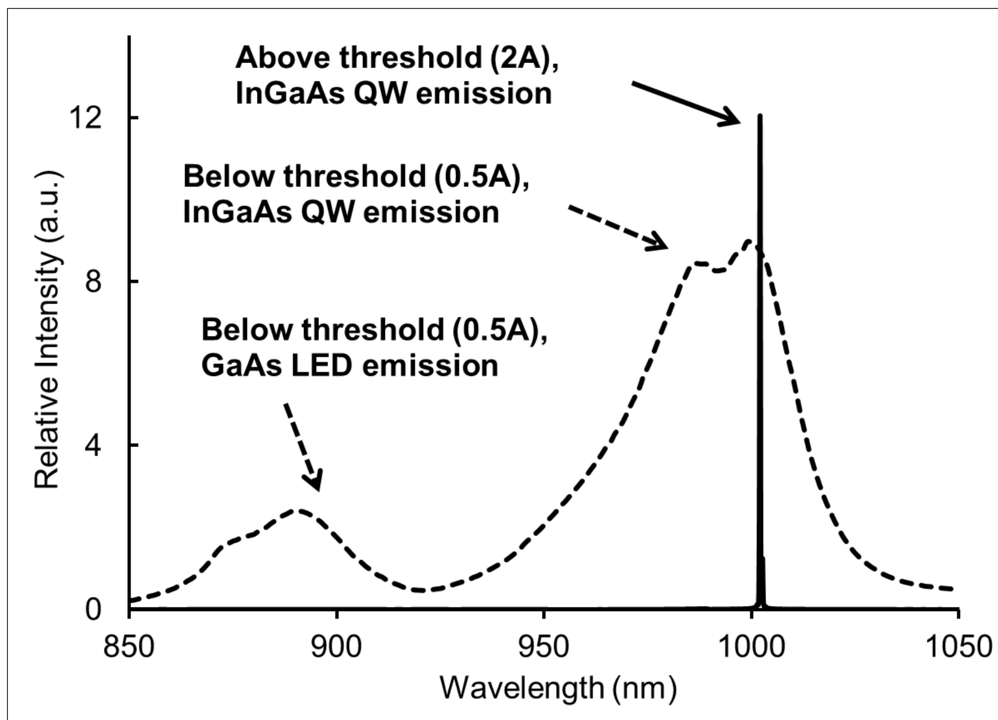

Figure 2-9 Electroluminescence measured from the chip at two different bias levels. The below threshold level at 0.5 A shows both the GaAs emission and the QW emission. At 2 A only laser emission from the QW occurs.

Numerous laser and LED designs had been investigated, with most showing room temperature laser operation. The light vs. current curve of one of the higher power integrated chips is shown in Figure 2-10. This sample has $Al_{0.02}Ga_{0.98}$ in the LED active region and three QWs in the laser structure, and 10 pairs of p mirror layers. The laser emission was measured

driving the chip continuous-wave with BeO heat sink, and the chip was p-side down mounted on the BeO heat sink with AuSn solder. The lasing threshold of the $In_{0.2}Ga_{0.8}As$ QW for a 120 μm wide electrical contact on the LED and 0.5 cm long cavity was measured to be 2 A under room temperature operation. The 2 A lasing threshold corresponds to a current density of 333 A/cm^2, which is only a factor of two higher than for an electrically injected p-n diode laser of similar waveguide and QW design, and contacting area. The slope efficiency of this device is 12%. There are two different slopes in the curve. The reason for decreased slope efficiency about 6A is probably due to heating of the device.

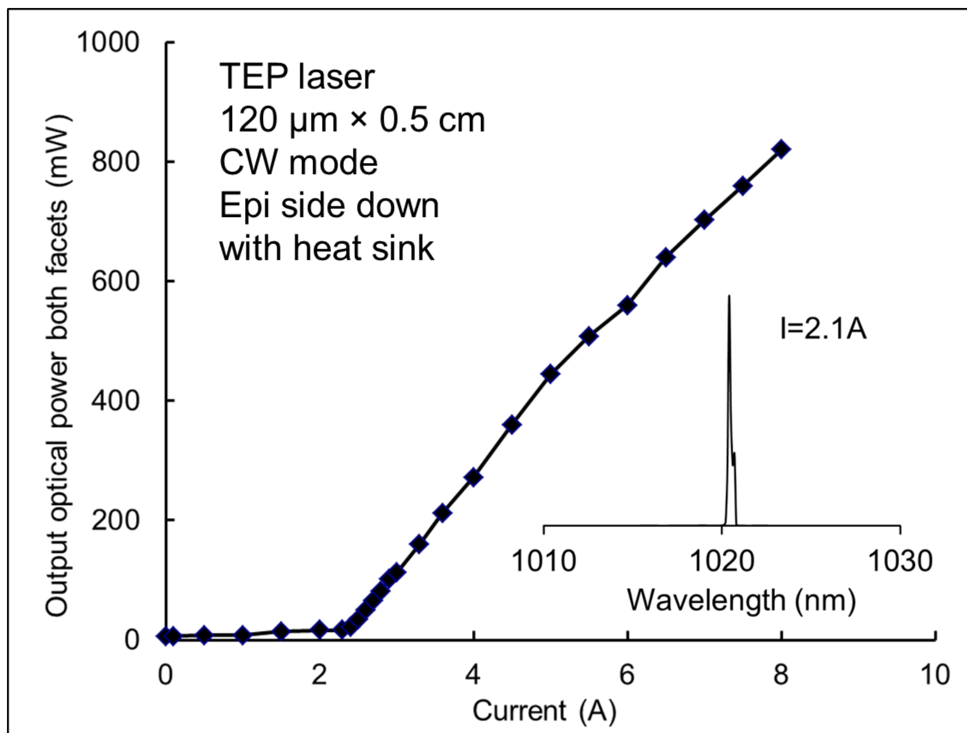

Figure 2-10 Light vs. current curve from the chip measured CW from both facets. Driving the LED electrically optically pumps the QW laser, which produces the laser emission shown in the inset. The stripe dimensions are 120 μm × 0.5 cm

We also note that optical absorption of the LED light by the laser waveguide is largely due to off-normal radiation modes due to their much larger solid angle of emission. Figure 2-11 demonstrates the optical power vs. injected current of two samples 665C and 665B with the same epi structure, but different device stripe width. The dimension of 665C and 665B are 120 μm × 0.5 cm and 50 μm × 0.5 cm, respectively.

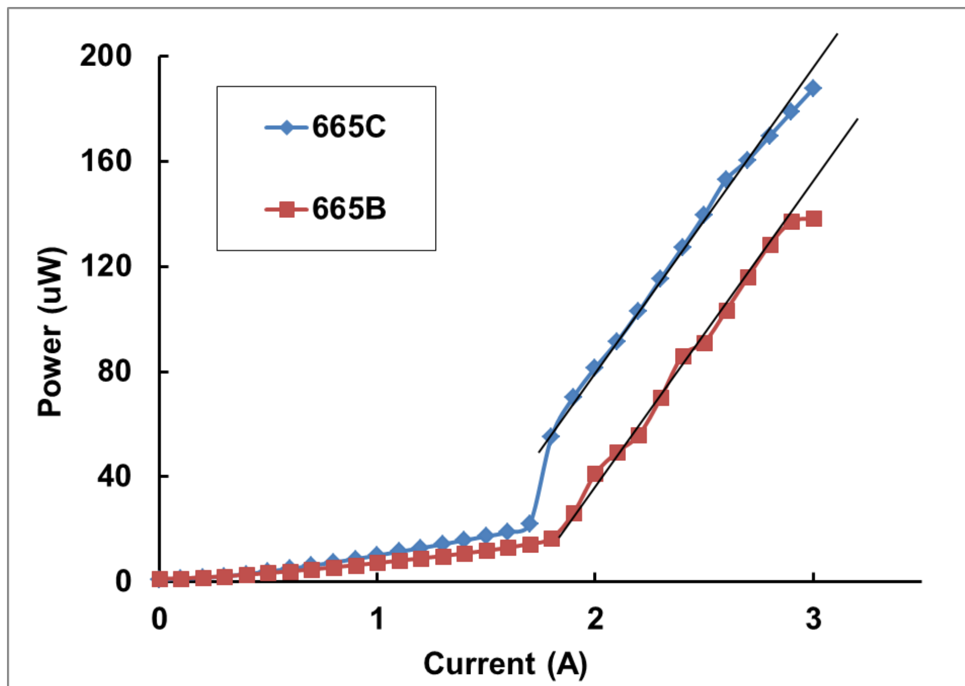

Figure 2-11 optical power vs. current data of two samples 665C (blue) and 665B (red), and their sizes are 120 μm × 0.5 cm and 50 μm × 0.5 cm, respectively.

The threshold of two samples calculated from the L-I curve are 600 A/cm^2 for 665B and 283 A/cm^2 for 665C. The threshold current density reduced by more than a factor of 2 by increasing the stripe width from 50 μm to 120 μm. It is because the off-normal radiation modes are more readily trapped between the LED and laser waveguide to increase absorption. Stripe

width is important because of edge effects in the radiation pattern of the LED. We have estimated this absorption in the current structures to be greater than 90%. Further optimization and simulation indicate that the absorption between the LED and laser QW active region could be increased potentially to as high as 98%.

2.5 Summary

We have shown that an internal LED optical pump that can be monolithically integrated with a semiconductor laser, and operated in a regime for which the LED can be optically absorbing while pumping the laser into CW operation at room temperature. Heat absorption is expected to result for sufficiently high internal quantum efficiency in the bulk LED, and this is currently being explored. Low internal optical loss is expected for the semiconductor laser due to elimination of p-doping from the cladding layers and removal of the need for hole injection, giving the prospect for increased efficiency and brightness from the semiconductor laser. It can be concluded from the efficiency expressions that the active region with low threshold and low loss is needed for higher efficiency of TEP lasers.

CHAPTER 3: TEP LASER WITH QUANTUM DOT ACTIVE REGION

3.1 Introduction

In order to improve TEP laser performance, we studied its efficiency in equation (2.6) – (2.8). It is really important to use QDs to be the active region of the laser due to its low threshold and loss internal loss. According to formula (2.6), low threshold of QD laser makes LED heat pump operate more effectively. When the current is reduced, TEP heat pump efficiency becomes more efficient in absorbing heat. In equation (2.7) and (2.8), low internal loss of QD laser enables the laser working more efficiently.

QD lasers have developed rapidly and they have unique laser characteristics compared with QW lasers [40]. The three-dimensional quantum confinement of the carriers results in discrete carrier energy level structure in the QD active region [41,42,43]. Their delta-function like density of the states enables more efficient injection of carriers and better suppression of excited states. Therefore, the QD laser diode offers low threshold current density, high differential gain [43,44], high characteristic temperature [40], and low value of alpha factor [45,46]. As mentioned in the previous chapter, the low threshold current density and low internal loss can increase laser diode cavity length, which maximize the output power without sacrificing its efficiency.

Transparency carrier density is the limitation of the internal loss in laser diode, which is defined as the density of carriers in the active region when the optical gain is zero. It is the minimal carrier density for which the material becomes transparent to photon energy above

bandgap. The value of the transparency carrier density depends on the intrinsic property of the active region, the heterojunction structure of active region and waveguide. As illustrated in Figure 3-1, QD active region has a discrete, delta-function like density of the states. A planar QW active region has a staircase like density of the states arriving in a continuous energy spectrum [47],[48]. The bulk active region has continuous density of states. The key difference in the density of states directly contributes to the significant reduction in the transparency current density of a QD active region compared to QW and bulk. The reduction in the transparency carrier density is at least one order of magnitude lower in the QD. The smaller carrier densities required to reach transparency in QD laser diode leads to a significant reduction in the threshold current density and optical internal loss.

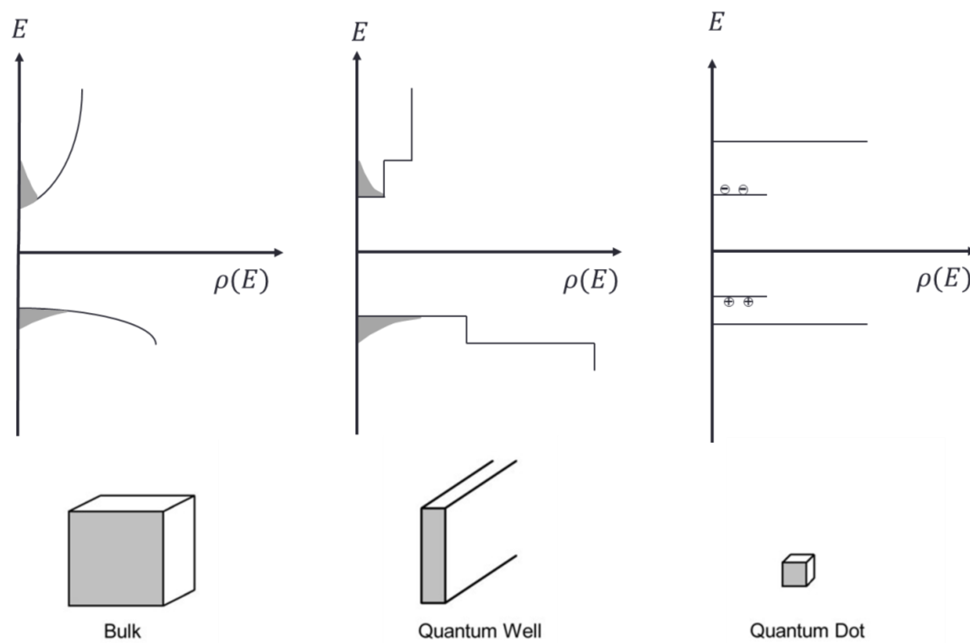

Figure 3-1 Density of states in active region of Bulk, QW and QD structure

QD laser was first realized in 1994 [40] by N. Kirstaedter *et al*. They grew $In_{0.5}Ga_{0.5}As$ on top of GaAs and its threshold current density was 950 A/cm^2 at RT and 120 A/cm^2 at 77 K. Liu *et al* achieved a threshold of 26 A/cm^2 at pulsed mode and room temperature by using "dot in a well" (DWELL) design, surpassing the threshold current density of QW laser [49]. In 2000 Park *et al* used increased dot density by sub monolayer depositions of In, Ga, and As on an $In_{0.09}Ga_{0.91}As$ buffer layer. The threshold of 19 A/cm^2 was reached at room temperature, CW operation [50]. Deppe *et al* in 2008 demonstrated the threshold current density of 11.7 A/cm^2 [51] at room temperature, p-up continuous operation. The laser had a single layer InAs QD active region with uncoated facets and 2 cm long cavity. Record low 8.8 A/cm^2 was achieved in the same structure with 2 cm long cavity, p-down mounted to BeO heatsink [52]. This is so far the lowest reported threshold current density for semiconductor edge emitting lasers.

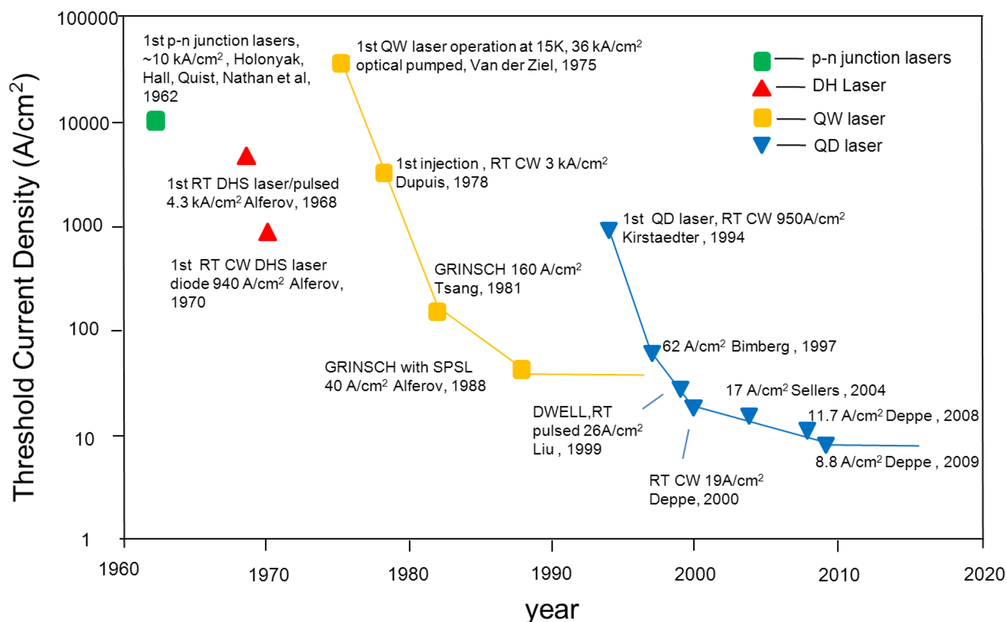

Figure 3-2 Development of EEL threshold current density

Theoretical study pointed out that internal loss of waveguide in high power semiconductor laser could be reduced with thicker waveguide and longer cavity [53]. Garbuzov *et al.* experimentally used broad waveguide structure reaching an internal loss of 1.3 cm^{-1} [54]. In an asymmetric heterostructure by Pikhtin *et al.*, they achieved 0.3 cm^{-1} with broad waveguide of 1.7 μm thick and 16 W CW operation [55]. The reason of shifting the optical mode to n-cladding is because free carrier absorption in n-type material is smaller, and the asymmetric optical mode has more overlap with n cladding. The resistive losses can therefore be reduced by increasing doping in p-type material. The limitation of internal loss is the free carrier scattering at the transparency carrier density in the active region. QD gain material is able to reach lasing condition with very low current density due to its low transparency carrier density. Consequently very low internal loss can be achieved in a QD laser diode. Experimentally, internal loss of ~0.25 cm^{-1} has been reported in the same record low threshold QD laser diode by Deppe *et al* [52]. This is the lowest internal loss ever reported for room temperature, CW operation laser diodes. In the following sections, the growth and design of a symmetric waveguide for low internal loss QD laser are demonstrated. The processing and fabrication of device are introduced, and the experimental data are presented.

3.2 QD Active Material Growth

The QD sample is grown on n-type GaAs substrate in MBE system. Quantum dots formation is a self-organized process. When material with larger lattice constant is deposited on

a substrate with smaller lattice constant, the first a few layers of atoms keep a coherent 2D growth while the strain in the layer builds up. When a critical thickness is reached, the materials on the top will partially release the strain by re-organizing their atoms into small island-shape clusters (quantum dots). This mode is named Stranski-Krastanow (SK) growth mode, illustrated in Figure 3-3.

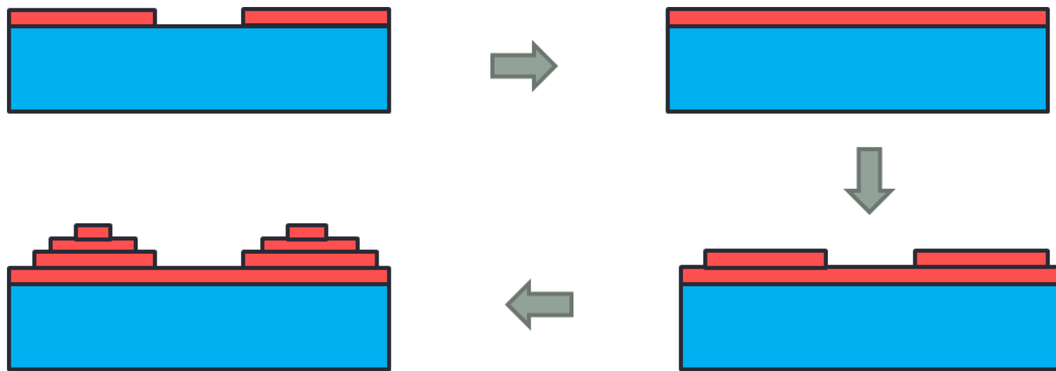

Figure 3-3 Stranski-Krastanow (SK) growth mode in forming quantum dots

Given proper substrate temperature and time for atoms to migrate on the growth surface, the self-organized quantum dots can be uniform in size, shape and distribution. Continuing deposition of materials lattice matched to the substrate will recover the growth surface and resume to 2D growth. The two fundamental factors affecting the formation of the quantum dots are the critical thickness, which depends on the lattice mismatch between the substrate and the quantum dot material, and the atoms mobility on the growth surface, which depend on many parameters such as the atom species, growth temperature and III/V flux ratio.

Figure 3-4 shows the Atomic Force Microscopy (AFM) images of InGaAs QD grown on GaAs substrate. The amount of InGaAs material deposited was carefully calibrated by the In and

Ga growth rate. The growth was terminated just after the quantum dots formed and the samples were taken out of the growth chamber for AFM characterization. The density, lateral size, height of the InGaAs QDs are 2×10^{10} cm^{-2}, 500 Å, and 60 Å.

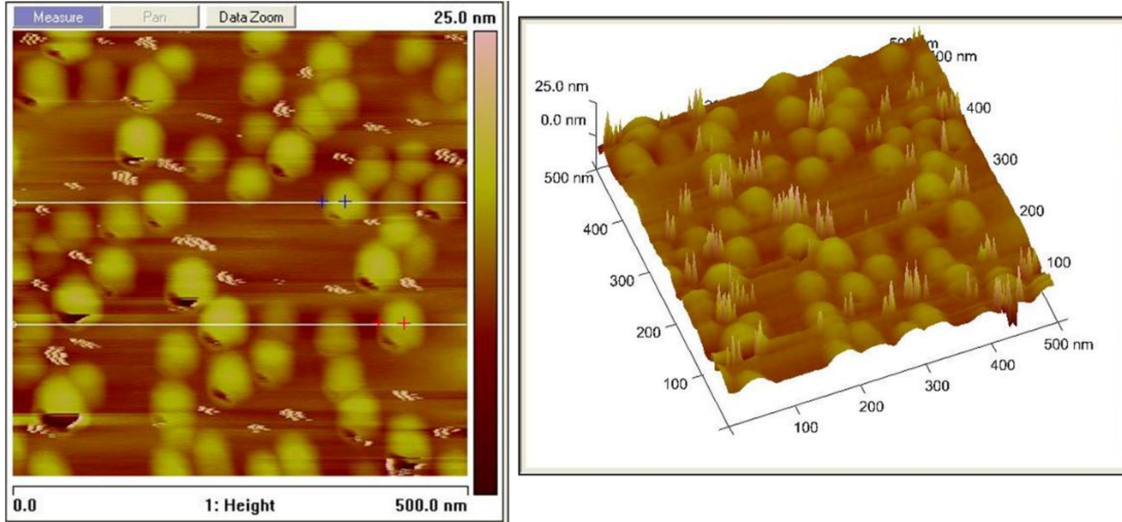

Figure 3-4 AFM scan of QD test growth. The growth of InGaAs on GaAs was terminated after the quantum dots formed. The density of the QDs is 2×10^{10} cm^{-2} (left). The lateral size, height of the QDs are 500 Å, and 60 Å respectively

3.3 QD EEL Fabrication and Characterization

A laser structure with the same QD active region was grown, and Figure 3-5 shows the schematic of QD broad area laser diode. The p and n cladding layers are $Al_{0.35}Ga_{0.65}As$. The p cladding is doped with beryllium at 1×10^{16} ~ 2×10^{17} cm^{-3}. The bottom n-cladding is doped with silicon at 1×10^{16} ~ 5×10^{17} cm^{-3}. The waveguide layer is $Al_{0.15}Ga_{0.85}As$ and its width is 2500 Å.

The active region consists of a single layer of InGaAs QDs operating at the emission wavelength of 980 nm.

The QD wafers were processed into broad area laser diodes. They were fabricated into stripes with width of 120 μm and cavity length of 0.5 cm. The p and n ohmic contacts were formed for carrier injection.

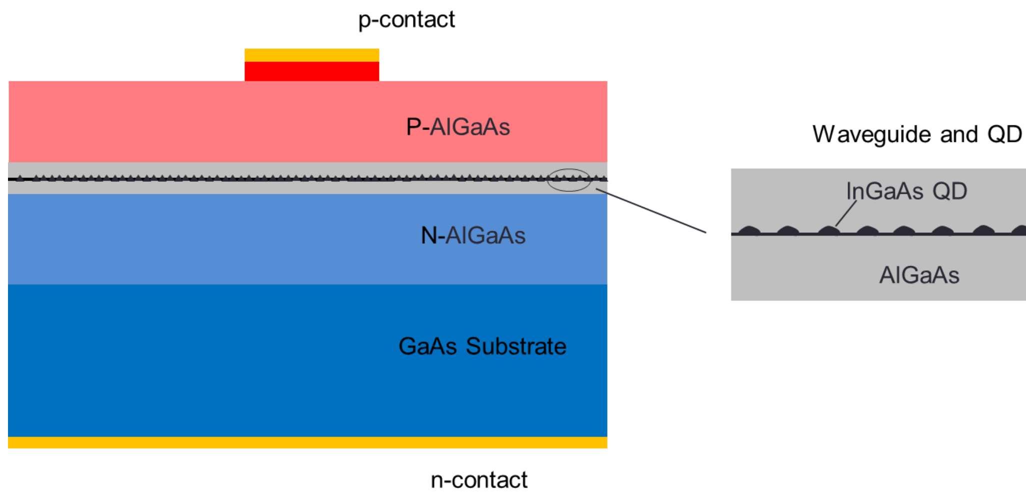

Figure 3-5 Schematic of QD broad area symmetric waveguide laser diode. The cladding layers are $Al_{0.35}Ga_{0.65}As$. The waveguide layer is $Al_{0.15}Ga_{0.85}As$. The active region uses the same QD structure as the test growth, a single layer of InGaAs QDs. The QD wafer is fabricated into 120 μm wide and 0.5 cm long laser diodes

The fabrication procedure of quantum dot laser wafer is demonstrated in Figure 3-6. 120 μm wide p metal stripes consist of 200 Å Chromium and 1500 Å Gold (Cr/Au) on top of the fresh epi-structure. After covering p metal contact and epi-structure with photoresist, the back side (n-side) of the wafer was etched and the damaged region during MBE crystal growth was etched off. The n metal contact of 200 Å Germanium and 1500 Å Gold (Ge / Au) were deposited

in thermal evaporator. The n metal alloyed with GaAs and Ohm contact was formed after the rapid thermal annealing (RTA) at 400 ℃ for 30 sec. The wafer was etched for 30 sec to form a shallow etched mesa ~1000 Å on the p side. We etched off the heavily doped top layers in this step to achieve current confinement.

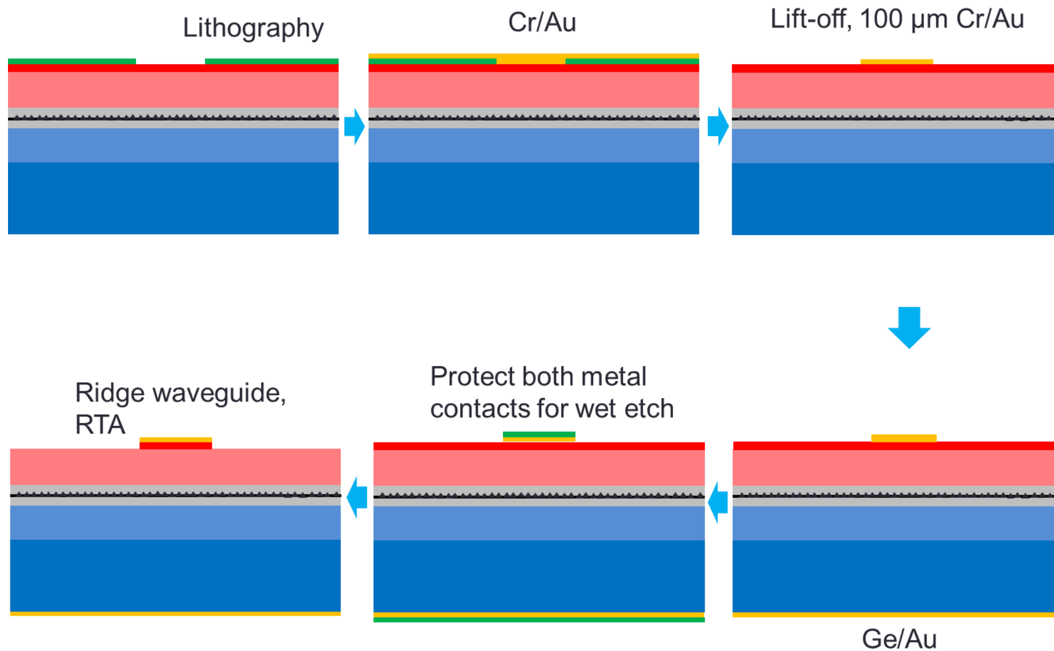

Figure 3-6 Fabrication procedure of the QD laser, the wafer was fabricated into stripes with 120 μm wide stripes and 0.5 cm long cavity. The p and n ohmic contacts were formed for carrier injection.

Figure 3-7 presents photoluminescence (PL) spectra of InGaAs QDs at 300 K and 77 K. The peak at 985 nm with full-width-at-half-maximum (FWHM) of 92.2 meV is corresponding to the QD ground-state transitions at the room-temperature. The PL peak shifts to the shorter wavelength at 946 nm as the temperature decreases. The wide ground state linewidth of 58.3 meV at 77 K is mainly due to inhomogeneous broadening from QD size non-uniformity.

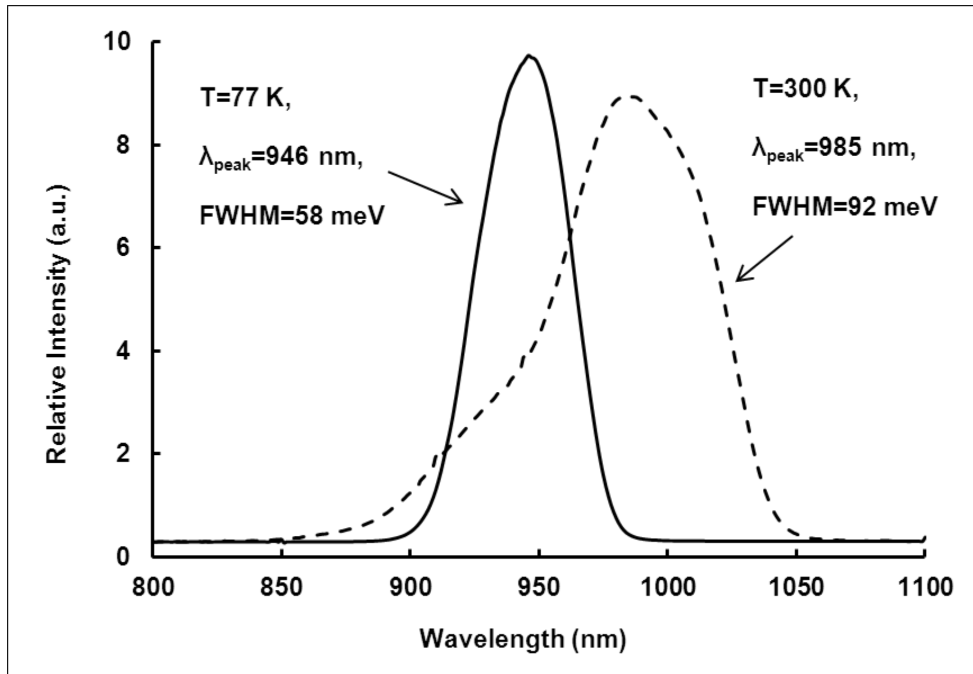

Figure 3-7 Photoluminescence spectra of a laser structure with the active region of 1 InGaAs QDs at 300 K and 77 K. The active region emitted at 985 nm with a FWHM of 92meV at 300K (dash line), and at 946nm with a FWHM of 58meV at 77K (solid line).

Figure 3-8 presents L-I curves for p-up mounted QD laser diode at room-temperature for CW operation of devices with 120 µm stripe width 0.3, 0.5, and 1 cm cavity length as cleaved. The testing of all devices terminated once the output power rolled over. The L-I curve shows the device with longer cavity length has lower threshold current density and can be driven to higher current, which is an indication of less heating. The maximum slope efficiency of each device is calculated in the inset.

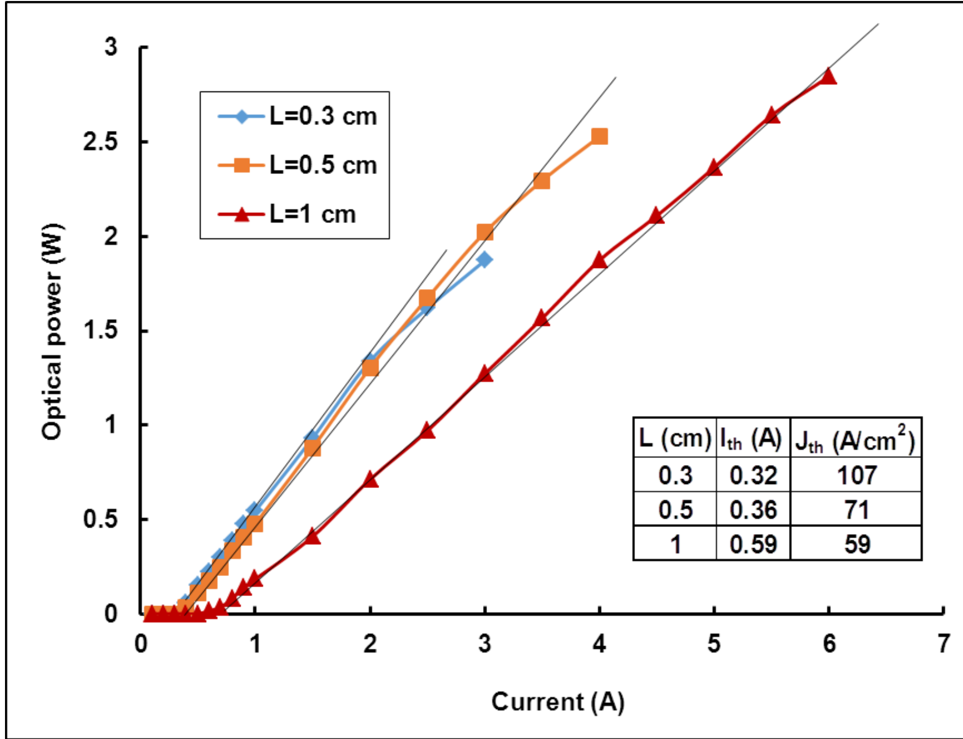

Figure 3-8 L-I curves for p-up mounted QD laser diodes at room-temperature for CW operation of devices with 100 µm stripe width, and 0.3, 0.5, and 1 cm cavity length. The inset shows the threshold current and threshold current density.

We are able to extract injection efficiency η_{inj} and internal optical loss α_i, with the slope efficiency of devices with different cavity lengths, , by using

$$\eta_s = \eta_{inj} \frac{ln(1/R_F)}{ln(1/R_F)+ln(1/R_B)+\alpha_i L} \quad (3.1)$$

in which front and back mirror reflectivity (R_F=R_B=0.3001). We are able to extrapolate injection efficiency of 81.26% and internal loss of 0.91 cm^{-1} from these data. Further optimization of the active region and waveguide to reduce optical loss are needed in future work.

Figure 3-9 shows the electroluminescence spectra at room-temperature for injected current density of 20, 60 and 80 A/cm^2 with stripe width of 100 µm, cavity length of 0.5 cm and p-up mounted on a copper block. The peak wavelength has blue shift from spontaneous emission to lasing stimulated emission. The spontaneous emission at 20 A/cm^2 around 988 nm is from ground state transitions and coincides with PL measurement. The central lasing wavelength of 967 nm is from excited state transitions. The low modal gain of the ground state leads to lasing at excited states and stimulated emission shifted to shorter wavelengt.

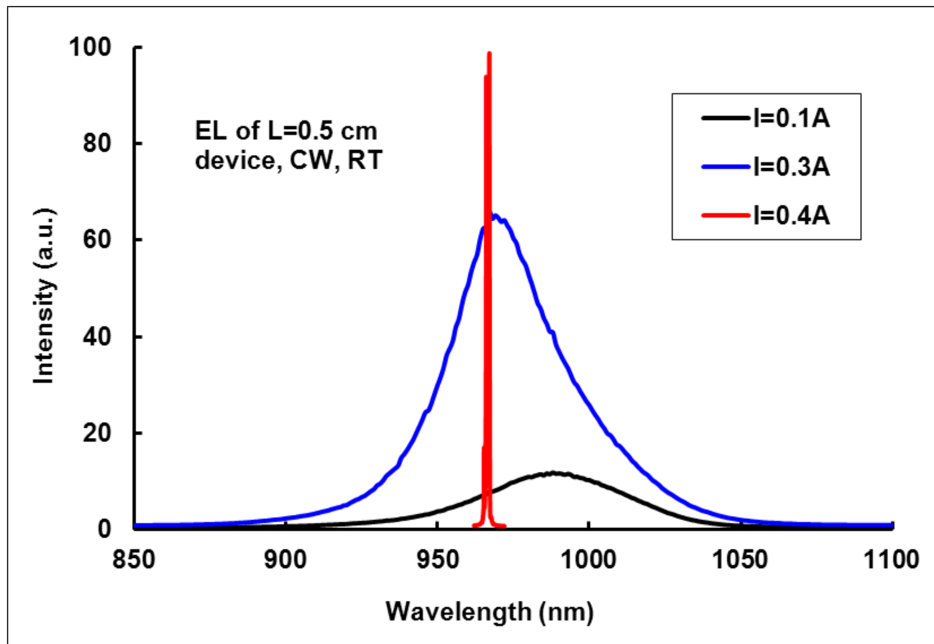

Figure 3-9 Electroluminescence spectra at room-temperature for different injected current density 0.1 A, 0.3 A, and 0.4 A below and above threshold

In order to study the critical thickness, emission wavelength, density and uniformity QDs, a few laser structures with different active regions were grown. An active region with more uniform and higher density of QDs is preferred, so that the gain at ground state is larger and this

will help suppress the excited states emission. Laser diodes will therefore benefit from the low carrier density in ground state due to low optical loss.

A laser sample was grown with less amount of InGaAs material 15 Å, and the waveguide and cladding structure remained the same. Figure 3-10 demonstrates its PL spectra at 300 K and 77 K. At 300 K, a peak is shown at 894 nm with FWHM of 26.4 meV. At 77 K, the peak is at 846 nm with FWHM 20.8 meV. The relatively narrow linewidth ~20 meV and short peak wavelength indicate that the active region is in fact a QW, and InGaAs material of 15Å has not reached the critical thickness of forming QD.

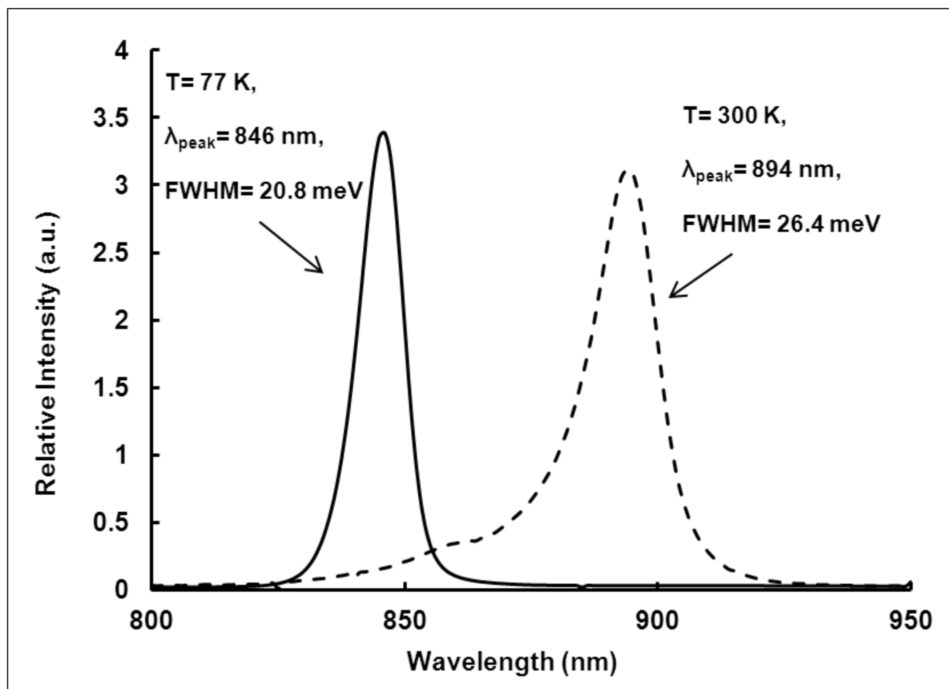

Figure 3-10 PL spectra of a laser structure with 15 Å InGaAs at 300 K and 77 K. The active region emitted at 894 nm with a FWHM of 26.4 meV at 300K (dash line), and at 846 nm with a FWHM of 20.8 meV at 77 K (solid line). The line width indicated the active region was a QW.

This ultra-thin QW active region with shorter emission wavelength at 910 nm is still interesting. The deep QW due to quantum effect will produce more confinement of carriers in the active region. Therefore the carriers in the waveguide and cladding layers thermalized from the active region would be greatly reduced, and the optical loss of this device will be minimized.

Figure 3-11 demonstrates the PL of another sample using 17.5 Å InGaAs materials in its active region. At 300 K, the peak is at 899 nm with FWHM of 24.6 meV, and at 77 K, the peak is at 852 nm with FWHM 22.3 meV. Compared with 15 Å InGaAs active region, this QW is shallower and its peak wavelength was red-shifted. The linewidth given from the sample at 77 K is likely from two-dimension QW, while the bump between 860 nm and 900 nm are probably the transition into zero-dimension quantum dots. It is almost certainly that the dots are beginning to form in regions, but apparently at very low density.

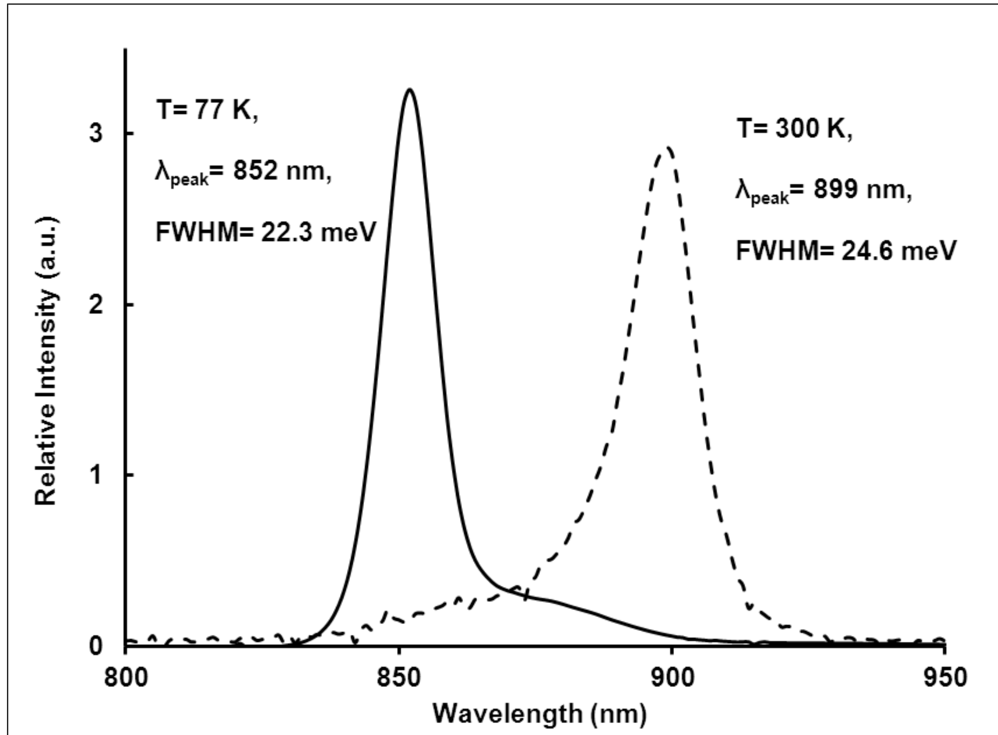

Figure 3-11 PL spectra of a laser structure with 17.5 Å InGaAs at 300 K and 77 K. The active region emitted at 899 nm with a FWHM of 24.6 meV at 300 K (dash line), and at 852 nm with a FWHM of 22.3 meV at 77 K (solid line). The bump between 860 nm and 900 nm are probably the transition from QW into quantum dots

Figure 3-12 demonstrates the PL of another test sample using 25 Å of InGaAs active materials. At 300 K, the peak wavelength is at 1010 nm with FWHM of 82.8 meV, and at 77 K, the peak is at 960 nm with FWHM 41.8 meV. Compared with 20 Å of InGaAs active region sample, this PL spectra have smaller linewidth, relatively higher intensity but longer peak wavelength. The narrower linewidth and higher intensity indicate the sizes of dots are more uniform and therefore the gain is larger. It can be concluded from the red-shift of the peak wavelength that the sizes of dots are larger, which brings the separation between first electron and hole states closer, and therefore emission wavelength longer.

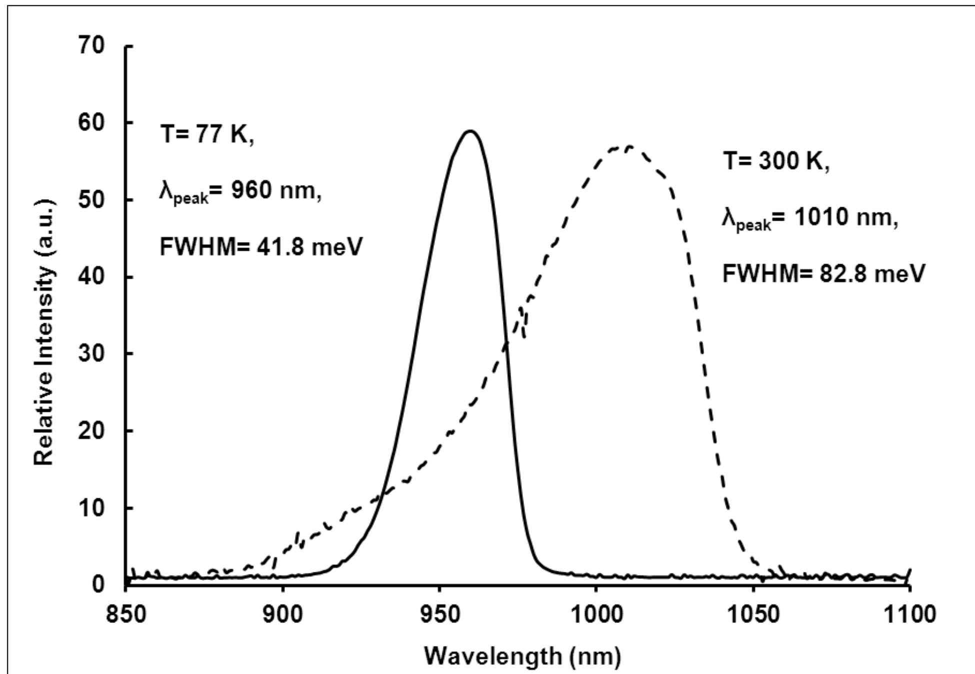

Figure 3-12 PL spectra of a laser structure with 25 Å InGaAs at 300 K and 77 K. The active region emitted at 960 nm with a FWHM of 41.8 meV at 300 K (dash line), and at 1010 nm with a FWHM of 82.8 meV at 77 K (solid line). The stronger emission and narrower linewidth indicate the sizes of quantum dots are more uniform and the gain is larger. The red-shift of peak wavelength is due to the larger size of quantum dots making separation of ground states of electrons and holes larger.

3.4 Possibility of Breaking Unity Efficiency in the Integrated Laser Chip with QDs as the TEP laser active region

We have shown that an internal LED optical pump that can be monolithically integrated with a semiconductor laser, and operated in a regime for which the LED can be optically absorbing while pumping the laser with CW operation at room temperature. Heat absorption is

expected for sufficiently high internal quantum efficiency in the bulk LED, and this is currently being explored. Low internal optical loss is expected for the semiconductor laser, due to elimination of doping from the cladding layers and removal of the need for hole and electron injection, giving the prospect for increased brightness and efficiency from the semiconductor laser. In order to further improve the efficiency and power of TEP laser, this section is focused on the efficiency calculation of TEP laser using QD as the active region material.

Our calculations in equation (2.6) indicate that the LED produces increased efficiency when operated at lower bias voltage, which produces a negative voltage defect relative the LED photon energy. It also produces increased heat absorption as the chip temperature increases. Therefore, the semiconductor laser must have low threshold and low optical loss to for the integrated chip to reach high efficiency. A model we simulated [56] also show that with sufficiently low threshold in the laser, and sufficiently small quantum defect between the LED pump and QW lasing transition, it may be possible for the integrated laser chip to enter the self-cooling regime with greater than unity power conversion efficiency.

This model includes the design of LED with an undoped 3 μm thick GaAs emitting at 875 nm that is clad by p and n doped $Al_{0.1}Ga_{0.9}As$ injection regions, and the laser with undoped InGaAs quantum dot layer in AlGaAs waveguide. QD laser is selected due to its low threshold current density and low internal loss. The lowest threshold current density ever reported for CW room-temperature laser diodes is 8.8 A/cm^2 [52] in a QD laser we designed and fabricated. The $Al_{0.1}Ga_{0.9}As$ and $Al_{0.2}Ga_{0.8}As$ waveguide layers are lightly doped. The threshold current density

and internal optical loss are calculated based on the laser structure with semiconductor physics and material parameters.

The calculation of optical mode profile in this laser waveguide is plotted Figure 3-14. It is a single lateral mode with confinement factor of 0.0102 in the QD active region. The active region of the QD laser is InGaAs which emits at 905 nm. 5 Å GaAs is designed on each side of the QD laser for material quality purposes. The waveguide of the laser is 0.6 μm $Al_{0.1}Ga_{0.9}As$, and the cladding layers of the waveguide are n-type 1 μm $Al_{0.2}Ga_{0.8}As$ on each side.

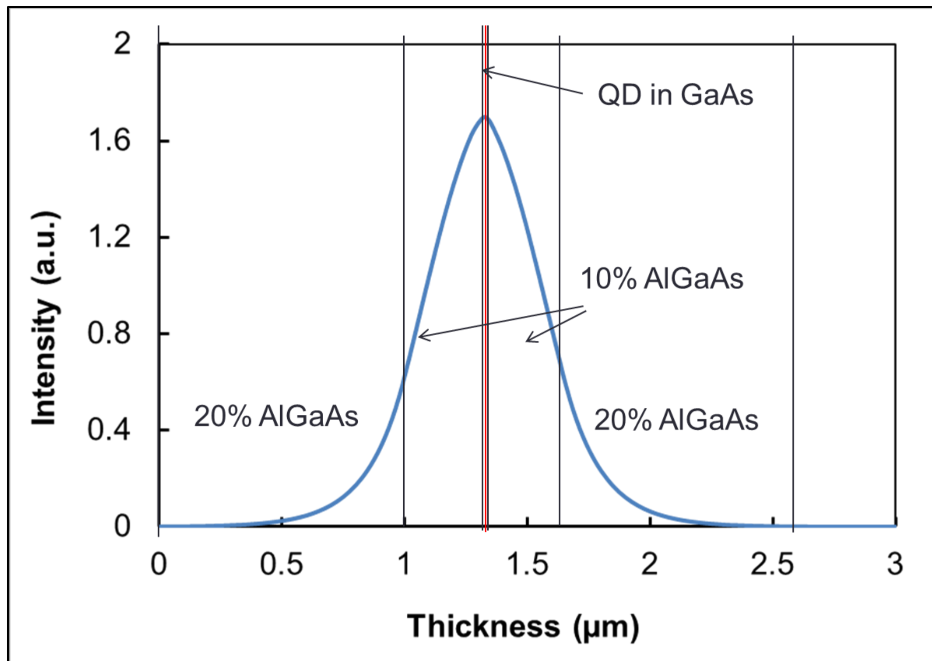

Figure 3-13 single optical mode in QD laser waveguide structure, the confinement factor in the active region is 0.0102

The parameters used for this equation are laser photon energy $\hbar\omega_L = 1.37\ eV$, LED pumping energy $\hbar\omega_{TEP} = 1.424\ eV$. The injection efficiency $\eta_{inj,Laser}$ and optical coupling

efficiency $\eta_{op,TEP-Laser}$ are estimated 99% respectively, since the interface between LED and laser is semiconductor – semiconductor, and the top and bottom mirrors will trap all LED light. The front and back mirror reflectivity R_F and R_B are 5% and 99% respectively. The threshold current density J_{th}, internal optical loss α_{WG} and junction voltage $V_{J,LED}$ could be simulated with the threshold of the lasing condition [57,58],

$$\frac{\omega}{Q} = v_g\left[\frac{1}{L}\,l\,n\left(\frac{1}{\sqrt{R_F R_B}}\right) + \alpha_{WG}\right] = \gamma_{sp,0}\frac{\pi^2 c^3}{n^3 {\omega_g}^2}\rho_{red}(\omega_g)\frac{\Gamma_{act}}{\Delta z}\cdot(f_e - f_h) \tag{3.1}$$

in which L is the cavity length, $v_g = 6.7\times10^7\ m/s$ is group velocity, refractive index $n = 3.35$ $\gamma_{sp,0} = 0.8\times10^9$ is spontaneous emission rate, f_e , f_h are Fermi probability of electrons and holes respectively, and can be related to carriers in QD by assuming ideal quantum dot with only one electron and hole sub-bands. N_{QD} is the density of quantum dots (cm^{-2}),

$$n_{QD} = N_{QD}\int_{E_{c,QD}}^{\infty}\rho_{QD}(E)dE\,\frac{1}{1+e^{\frac{E-F_e}{kT}}} = 2N_{QD}\cdot f_e(E_{c,QD}) \tag{3.2}$$

$$p_{QD} = N_{QD}\int_{-\infty}^{E_{v,QD}}\rho_{QD}(E)dE\cdot\left(1-\frac{1}{1+e^{\frac{E-F_h}{kT}}}\right) = 2N_{QD}\cdot\left(1-f_h(E_{v,QD})\right) \tag{3.3}$$

Carrier density thermalized into GaAs and AlGaAs waveguide layer can be estimated with carrier density in InGaAs QD, and band offset between GaAs and InGaAs, assuming the Fermi energy level at the QD/GaAs interface are the same,

$$n_{GaAs} = 2\left(\frac{m_{e,GaAs}kT}{2\pi\hbar^2}\right)^{\frac{3}{2}} e^{-\frac{E_{c,QD}-F_e}{kT}} e^{\frac{E_{c,QD}-E_{c,GaAs}}{kT}} = 2\left(\frac{m_{e,GaAs}kT}{2\pi\hbar^2}\right)^{\frac{3}{2}}\frac{1}{\frac{2N_{QD}}{n_{QD}}-1} \tag{3.4}$$

$$p_{GaAs} = 2\left(\frac{m_{h,GaAs}kT}{2\pi\hbar^2}\right)^{\frac{3}{2}} e^{\frac{E_{v,QD}-F_h}{kT}} e^{\frac{E_{v,GaAs}-E_{v,QD}}{kT}} = 2\left(\frac{m_{h,GaAs}kT}{2\pi\hbar^2}\right)^{\frac{3}{2}} \frac{1}{\frac{2N_{QD}}{p_{QD}}-1} e^{\frac{E_{v,GaAs}-E_{v,QD}}{kT}}$$

(3.5)

where n_{GaAs} and p_{GaAs} are the election and hole concentration in GaAs layer, n_{QD} and p_{QD} are the carrier density in QD. $N_{QD}{\sim}3 \times 10^{10} cm^{-2}$ is the density of QD. $m_{e,GaAs}$ and $m_{h,GaAs}$ are electron and hole masses. The electrons and holes in AlGaAs cladding layers could be estimated with the same method. The spontaneous emission current at the threshold is [26],

$$J_{Spon} = 2qN_{QD}\gamma_{sp,0} \cdot [f_e(1-f_h)] \tag{3.6}$$

With estimated carrier density in QD and waveguide, the optical loss of QD laser structure can also be simulated, as shown in (2.4) and (2.5). Therefore the threshold carrier density and current density for different cavity length can be calculated, with threshold condition. Table 3-1 shows the results of internal loss and threshold current density of devices with different cavity length,

Table 3-1 loss and threshold calcualtion with different cavity length

Cavity length (cm)	Threshold current density (A/cm^2)	Total loss (1/cm)
0.2cm	7.677	0.073
0.4cm	5.266	0.046
0.6cm	4.545	0.043

The power conversion efficiency of the 0.4 cm device vs. injected current density is plotted in Fig 3-14. The maximum efficiency is just above unity at 234 A/cm^2, and the efficiency of LED at this current is 110.3%. The calculated maximum efficiency of the integrated chip is above 100%, meaning the optical output of the laser the laser chip exceeds the electric and heat is drawn from the thermal contact and heat sink. Figure 3-15 shows the calculated efficiency of LED heat pump at the same current is 110.3%. As expected, the LED has higher efficiency with lower injected current and applied voltage.

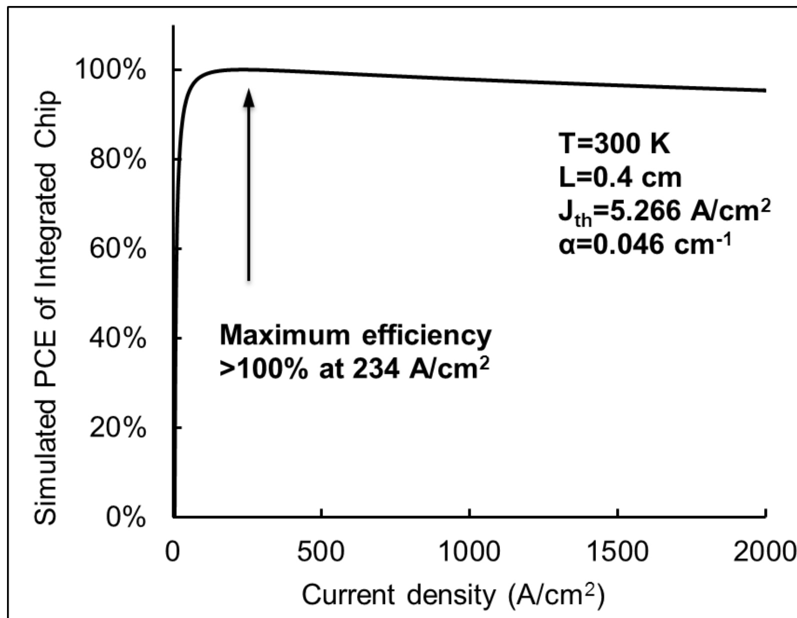

Figure 3-14 Simulated power conversion efficiency of integrated chip

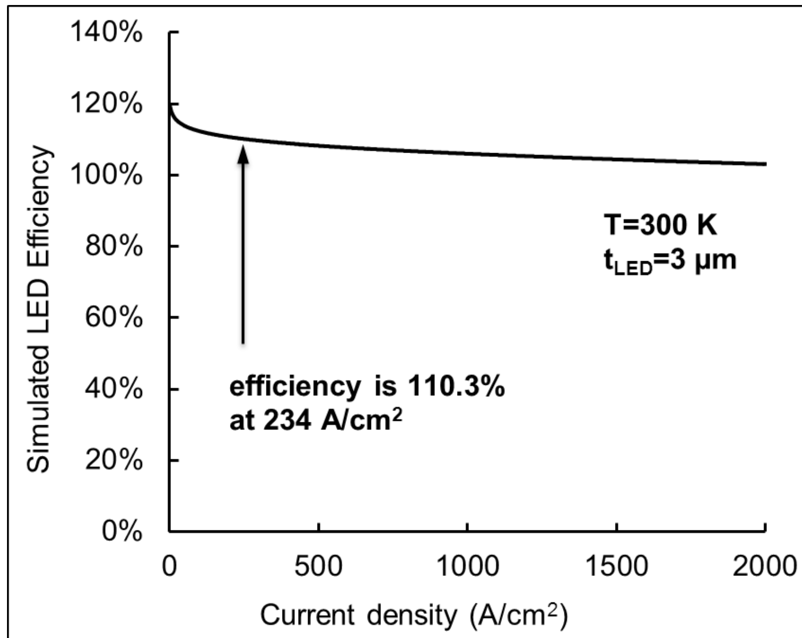

Figure 3-15 Power conversion efficiency of integrated chip (left) and LED (right) of a device with 0.4 cm cavity length

3.5 Summary

This chapter discussed the importance of QDs as the active region of TEP laser. Single QD layer active region due to its unique structure, can have low transparency density carrier, which gives the low loss and threshold. In this work, S-K growth mode was used to form self-organized QDs. The characterizations of QD EEL with symmetric waveguide were demonstrated. The threshold of a 1 cm long device is 59 A/cm^2 at room temperature, and its estimated internal loss is 0.91 cm^{-1}. Improvement of QDs active region were demonstrated and the growth of more uniform QDs are achieved. In the future, optimization of waveguide structure

and engineering of active region are needed to further improvement of TEP laser performance. Simulations also show that with sufficiently low threshold in the laser and small quantum defect between the LED pump and QW lasing transition, it is possible for the integrated laser chip to enter the self-cooling regime with greater than unity power conversion efficiency.

CHAPTER 4: SUMMARY AND FUTURE WORK

A semiconductor laser monolithically integrated with an LED optical pump was presented. The LED could also work as a heat pump with sufficiently high internal quantum efficiency. Due to the elimination of doping from the cladding layers and removal of the need for carriers electrical injection, low internal optical loss is expected from the semiconductor laser. Experimental results showed that the integrated laser chip was lasing at 300 A/cm^2, and the slope efficiency was 12%. In order to further improve performance of TEP laser, QDs as the active region of TEP EEL was studied. The physical property of QD active region is described. The importance of using QD in the active region in terms of low threshold and low optical loss was well understood. The crystal growth of self-organized QD was explained. The symmetric waveguide laser structure was used and the fabrication procedure was detailed. The device with no heat sink was tested at room temperature. A device with 1 cm cavity length and 100 µm width had a threshold of 59 A/cm^2 and internal loss of 0.92 cm^{-1}. Further optimization of QD growth were discussed. Characterization of a few active region indicated the critical thickness of InGaAs QDs growth is about 17.5 Å. Simulations also showed that with sufficiently low threshold in the laser, and sufficiently small quantum defect between the LED pump and QW lasing transition, it was possible for the integrated laser chip to enter the self-cooling regime with greater than unity power conversion efficiency. Future work includes growth of QD active region with better performance, and design and growth of high quality laser waveguide.

LIST OF REFERENCES

[1] J. Tauc, Czech. "The share of thermal energy taken from the surroundings in the electro-luminescent energy radiated from a p-n junction" J. Phys. 7, 275 (1957).

[2] A. Weinstein "Thermodynamic limitation on the conversion of heat into light" J. Opt. Soc. Am. 50, 597 (1960).

[3] R.J. Keyes and T.M. Quist, "Recombination radiation emitted by GaAs," Proc. IRE 50, 1822 (1962).

[4] G.C. Dousmanis, C.W. Mueller, H. Nelson, and K.G. Petzinger, "Evidence of refrigerating action by means of photon emission in semiconductor diodes," Phys. Rev. 133, A316 (1964).

[5] I. Schnitzer, E. Yablonovitch, C. Caneau, and T.J. Gmitter, "Ultrahigh spontaneous emission quantum efficiency, 99.7% internally and 72% externally, from AlGaAs/GaAs/AlGaAs double heterostructures," Appl. Phys. Lett. 62, 131 (1993).

[6] P. Berdahl, "Radiant refrigeration by semiconductor diodes," J. Appl. Phys. 58, 1369 (1985).

[7] K.C. Lee and S.T. Yen, "Photon recycling effect on electroluminescent refrigeration," J. Appl. Phys. 111, 014511 (2012).

[8] O. Heikkila, J. Oksanen, and J. Tulkki, "The challenge of unity wall plug efficiency: The effects of internal heating on the efficiency of light emitting diodes" J. Appl. Phys. 107, 033105 (2010).

[9] S.-Q. Yu et al., “Fundamental mechanisms of electroluminescence refrigeration in heterostructure light-emitting diodes” Proc. SPIE Int. Soc. Opt. Eng. 6486, 648604 (2007).

[10] S.-T. Yen and K.-C. Lee, “Analysis of heterostructures for electroluminescent refrigeration and light emitting without heat generation” J. Appl. Phys. 107, 054513 (2010).

[11] P. Han, K.-J. Jin, Y.-L. Zhou, H.-B. Lu, and G.-Z. Yang, “Numerical designing of semiconductor structure for optothermionic refrigeration” J. Appl. Phys. 101, 014506 (2007).

[12] A. G. Mal’shukov and K. A. Chao, “Opto-Thermionic Refrigeration in Semiconductor Heterostructures” Phys. Rev. Lett. 86, 5570 (2001).

[13] J. Oksanen and J. Tulkki, “Effects of photon transport, emission saturation, and reflection losses on thermophotonic cooling” Proc. SPIE Int. Soc. Opt. Eng. 7951, 79510H (2011).

[14] P. Santhanam, D.J. Gray, and R.J. Ram, "Thermoelectrically Pumped Light-Emitting Diodes Operating Above Unity Efficiency," Phys. Rev. Lett. 108, 097403 (2012)

[15] P. Santhanam, D. Huang, R. J. Ram, M. A. Remennyi and B. A. Matveev, “Room temperature thermo-electric pumping in mid-infrared light-emitting diodes” Appl. Phys. Lett. 103, 183513 (2013).

[16] R. N. Hall, G. E. Fenner, J. D. Kingsley, T. J. Soltys, and R. O. Carlson, Phys. Rev. Lett., vol. 9, p. 366, 1962.

[17] M. I. Nathan, W. Dumke, G. Burns, F. H. Dill Jr., and G. Lasher, Appl.Phys. Lett., vol. 1, p. 62, 1962

[18] N. Holonyak Jr. and S. F. Bevacqua, Appl. Phys. Lett., vol. 1, p. 82, 1962.

[19] T. M. Quist, R. H. Rediker, R. J. Keyes, W. E. Krag, B. Lax, A. L. McWhorter, and H. J. Zeigler, Appl. Phys. Lett., vol. 1, p. 91, 1962.

[20] I. Hayashi, M. B. Panish, W. Foy, and S. Sumski, Appl. Phys. Lett., vol.17, p. 109, 1970.

[21] Zh. I. Alferov, V. M. Andreev, D. Z. Garbuzov, Yu. V. Zhilyaev, E. P. Morozov, E. L. Portnoi, and V. G. Trofim, Sov. Phys. Semicond., vol. 4, p. 1573, 1971.

[22] D. R. Scifres, C. Lindstrom, R. D. Burnham,W. Streifer, and T. L. Paoli, Electron. Lett., vol. 19, p. 169, 1983.

[23] M. Sakamoto, D. F. Welch, H. Yao, J. G. Endriz, and D. R. Scifres, Electron. Lett., vol. 26, p. 729, 1990.

[24] E. Wolak, M. Sakamoto, J. Endriz, and D. R. Scifres, LEOS ’92 Digest, 1992, Paper No. DLTA 5.1, p. 175.

[25] D. K.Wagner, R. G.Waters, P. L. Tihanyi, D. S. Hill, A. J. Roza Jr., H. J. Vollmer, and M. M. Leopold, IEEE J.Quantum Electron., vol. QE-24, p. 1258, 1988.

[26] D. F.Welch, B. Chan,W. Streifer, and D. R. Scifres, Electron. Lett., vol. 24, p. 113, 1988.

[27] G. L. Harnagel, P. S. Cross, D. R. Scifres, and D. Worland, Electron.Lett., vol. 2, p. 231, 1986.

[28] D. P. Bour and A. Rosen, J. Appl. Phys. 66, 2813 (1989).

[29] D. Botez, L. J. Mawst, A. Bhattacharya, L. Lopez, J. Li, V. P. Iakovlev, G. I. Suruceanu, A. Caliman, and A. V. Syrbu, Electron. Lett. 32, 2012 (1996).

[30] M. A. Emanuel, N. W. Carlson, and J. K. Skidmore, IEEE Photonics Technol. Lett. 8, 1291 (1996).

[31] R. G. Waters, D. K. Wagner, D. S. Hill, P. L. Tihanyi, and B. J. Vollmer, Appl. Phys. Lett. 51, 1318 (1987).

[32] D. Z. Garbuzov, J. H. Abeles, N. A. Morris, P. D. Gardner, A. R. Triano, M. G. Harvey, D. B. Gilbert, and J. C. Connolly, Proc. SPIE 2682, 20 (1996)

[33] Wang, Jun, Barry Smith, Xiaomin Xie, Xinqiao Wang, and Geoffrey T. Burnham. "High-efficiency diode lasers at high output power." Applied physics letters 74, no. 11 (1999): 1525-1527

[34] Crump, Paul, Jun Wang, Trevor Crum, Suhit Das, Mark DeVito, Weimin Dong, Jason Farmer et al. "> 360 W and > 70% efficient GaAs-based diode lasers." In Lasers and Applications in Science and Engineering, pp. 21-29. International Society for Optics and Photonics, 2005

[35] Sonia Quader “HIGH POWER HIGH EFFICIENCY ELECTRON-HOLE AND UNIPOLAR QUANTUM DOT LASERS” University of Texas at Austin (2007).

[36] B.S. Ryvkin, and E.A. Avrutin, “ Effect of carrier loss through waveguide layer recombination on the internal quantum efficiency in large-optical-cavity laser diodes,” J. of Appl. Phys., Vol. 97, pp.113106 (2005).

[37] N.A. Pikhtin, S.O. Slipchenko, Z.N. Sokolova, and I.S. Tarasov, “Internal Optical loss in semiconductor lasers,” Semiconductors, Vol. 38, no. 3, pp.360-367 (2004).

[38] V.M. Ustinov, A. E. Zhukov, A.Y. Egorov, and N.A.Maleev, “Quantum Dot Lasers,” Oxford University Press (2003).

[39] Liu, X.; Zhao, G.; Zhang, Y.; Deppe, D.G., "Optoelectronic Chip Based on a Laser Integrated with a Thermoelectrophotonic Heat Pump," Compound Semiconductor Integrated Circuit Symposium (CSICS), 2012 IEEE , vol., no., pp.1,4, 14-17 Oct. 2012. doi: 10.1109/CSICS.2012.6340117

[40] Kirstaedter, N.; Ledentsov, N.N.; Grundmann, M.; Bimberg, D.; Ustinov, V.M.; Ruvimov, S.S.; Maximov, M.V.; Kop'ev, P.S.; Alferov, Zh.I; Richter, U.; Werner, P.; Gosele, U.; Heydenreich, J., "Low threshold, large To injection laser emission from (InGa)As quantum dots," Electronics Letters , vol.30, no.17, pp.1416,1417, 18 Aug 1994. doi: 10.1049/el:19940939

[41] Arakawa, Y. and Sakaki, H., "Multidimensional quantum well laser and temperature dependence of its threshold current," Applied Physics Letters, 40, 939-941 (1982), DOI:http://dx.doi.org/10.1063/1.92959

[42] Asada, M.; Miyamoto, Y.; Suematsu, Y., "Gain and the threshold of three-dimensional quantum-box lasers," Quantum Electronics, IEEE Journal of , vol.22, no.9, pp.1915,1921, Sep 1986. doi: 10.1109/JQE.1986.1073149

[43] Vahala, K.J., "Quantum box fabrication tolerance and size limits in semiconductors and their effect on optical gain," Quantum Electronics, IEEE Journal of , vol.24, no.3, pp.523,530, Mar 1988. doi: 10.1109/3.157

[44] Arakawa, Y.; Yariv, A, "Quantum well lasers--Gain, spectra, dynamics," Quantum Electronics, IEEE Journal of , vol.22, no.9, pp.1887,1899, Sep 1986 doi: 10.1109/JQE.1986.1073185

[45] Bimberg, D.; Kirstaedter, N.; Ledentsov, N.N.; Alferov, Zh.I; Kop'ev, P. S.; Ustinov, V.M., "InGaAs-GaAs quantum-dot lasers," Selected Topics in Quantum Electronics, IEEE Journal of , vol.3, no.2, pp.196,205, Apr 1997. doi: 10.1109/2944.605656

[46] Newell, T.C.; Bossert, D.J.; Stintz, A; Fuchs, B.; Malloy, K.J.; Lester, L.F., "Gain and linewidth enhancement factor in InAs quantum-dot laser diodes," Photonics Technology Letters, IEEE , vol.11, no.12, pp.1527,1529, Dec. 1999. doi: 10.1109/68.806834

[47] Asryan, L. V. and Suris, R. A., "Inhomogeneous line broadening and the threshold current density of a semiconductor quantum dot laser," Semicond. Sci. Technol. , vol. 11,p. 554, 1996.

[48] Grundmann, M. and Bimberg, D., "Gain and threshold of quantum dot lasers: Theory and comparison to experiments," Jpn. J. Appl. Phys., vol. 36, pp. 4181-4189, 1997.

[49] Liu, G. T., Li, H., Malloy, J., and Lester, L. F., "Extremely low room-temperaturethreshold current density diode lasers using InAs dots in In0.15Ga0.85As quantum well,"Electron. Lett., vol. 35, pp. 1163-1164, 1999.

[50] Park, G., Schekin, O. B., Huffaker, D. L., and Deppe, D. G., "1.3-μm quantum-dot laser," IEEE Photonics Technol. Lett., vol. 12, pp. 230-232, 2000.

[51] Freisem, S., Ozgur, G., Shavritranuruk, K., Chen, H., and Deppe, D.G.: “Very low threshold current density continuous wave quantum dot laser,” Electron. Lett., 2008, 44, pp. 679–680

[52] Deppe, D.G.; Shavritranuruk, K.; Ozgur, G.; Chen, H.; Freisem, S., "Quantum dot laser diode with low threshold and low internal loss," Electronics Letters , vol.45, no.1, pp.54,56, January 1 2009. doi: 10.1049/el:20092873

[53] Pikhtin, N. A., Slipchenko, S. O., Sokolova, Z. N., and Tarasov, I. S., "Internal Optical Loss in Semiconductor Lasers," Semiconductor vol. 38, pp. 360-367, 2004.

[54] Garbuzov, D.; Xu, L.; Forrest, S.R.; Menna, R.; Martinelli, R.; Connolly, J.C., "1.5 μm wavelength, SCH-MQW InGaAsP/InP broadened-waveguide laser diodes with low internal loss and high output power," Electronics Letters , vol.32, no.18, pp.1717,, 29 Aug 1996 doi: 10.1049/el:19961098

[55] Slipchenko, S. O., Vinokurov, D. A., Pikhtin, N. A., Sokolova, Z. N., Stankevich, A. L.,Tarasov, I. S., and Alferov, Z. I., "Ultralow internal optical loss in seperate-confinementquauntum well heterostructures," Semiconductor, vol. 38, pp. 1430-1439, 2004..

[56] X. Liu, Y. Zhang, G. Zhao, and D. Deppe, "Possibility for Breaking the Unity Efficiency Barrier: Semiconductor Laser Optically Pumped by an Integrated Light Emitting Diode," in CLEO: 2013, OSA

[57] D.G. Deppe, D.L.Huffaker, Z.Zou, G.Park, O.B.Shchekin, "Spontaneous emission and threshold characteristics of 1.3-μm InGaAs-GaAs quantum-dot GaAs-based lasers", Quantum Electronics, IEEE Journal of 1999

[58] Z. Zou, O. B. Shchekin, G. Park, D. L. Huffaker, and D. G. Deppe, "Threshold temperature dependence of lateral cavity quantum dot lasers", IEEE Photon. Technol. Lett., vol. 10, pp.1673 -1675 1998.